Solar Data

Heliophysics Summer School, August 3rd 2022

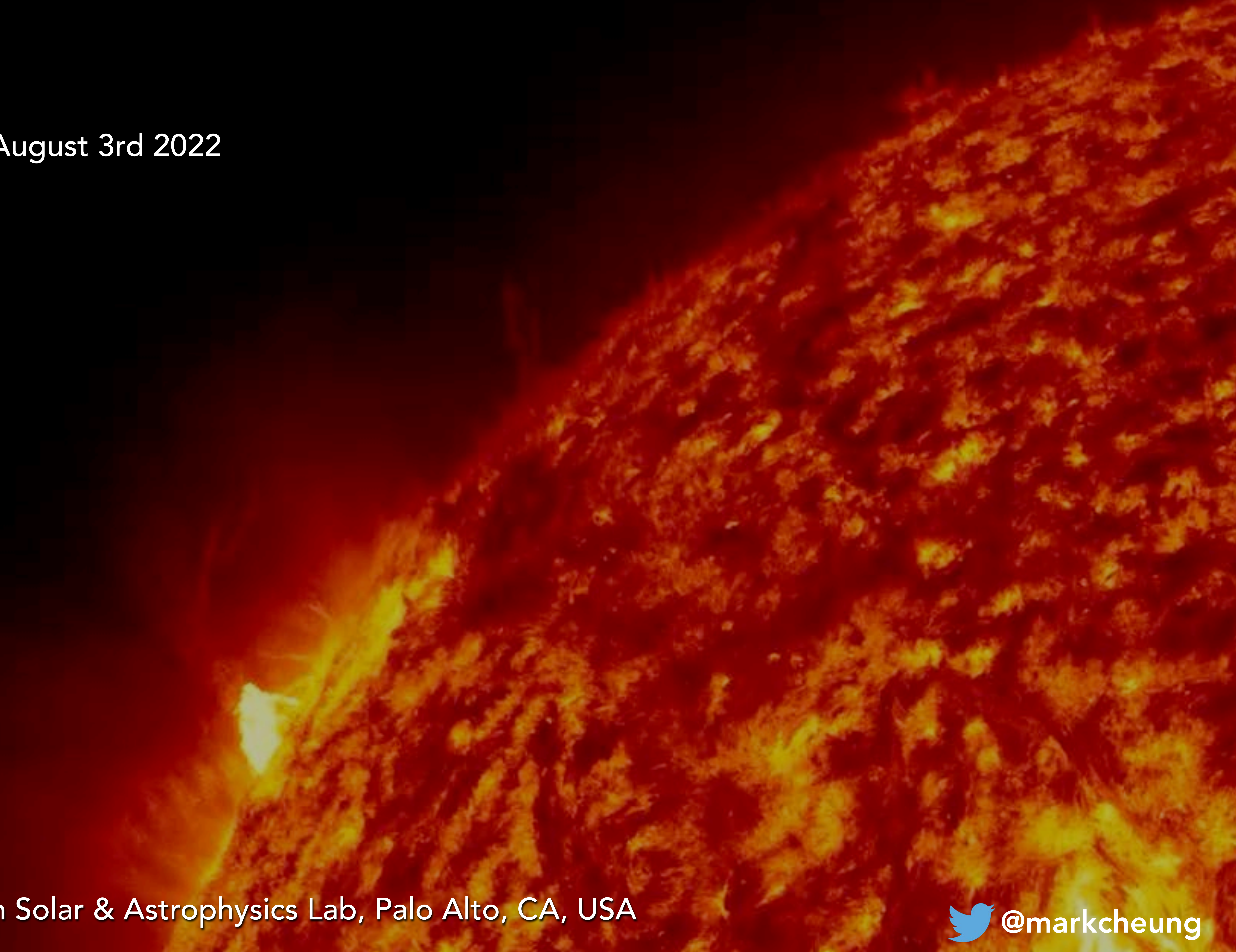

Mark Cheung, Lockheed Martin Solar & Astrophysics Lab, Palo Alto, CA, USA

@markcheung

Solar Astronomy 101

Most Salient Observational Features about the Sun

- It rotates, but not as a solid body. The equator rotates faster than the poles (use helioseismology to probe the interior).
- It has sunspots. The number of sunspots waxes and wanes with an eleven year cycle.
- Magnetic fields pervade the entire Sun.
- The Sun is a panchromatic astrophysical object.

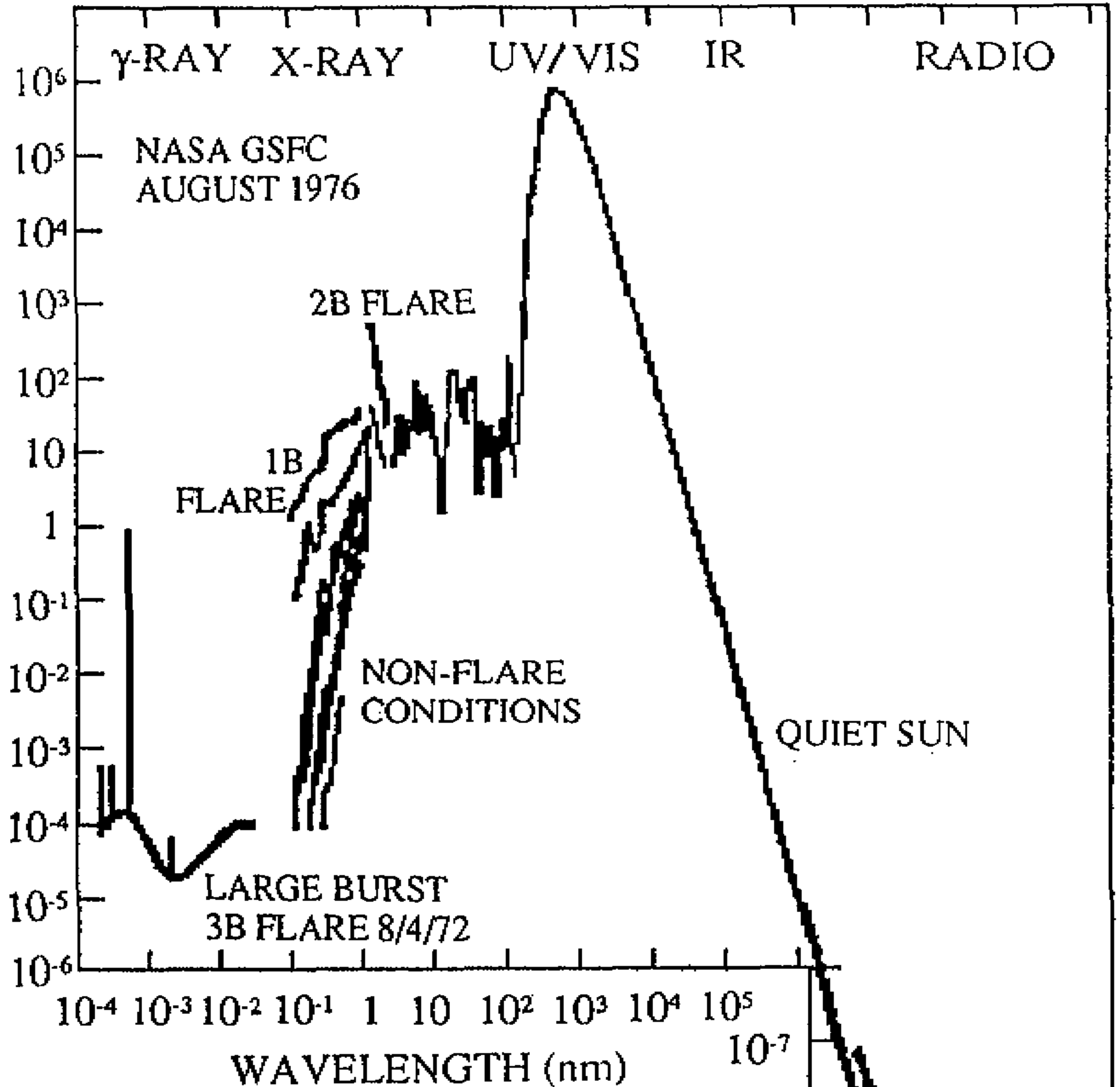
γ-RAY
X-RAY
UV/VIS
IR
RADIO
NASA GSFC
AUGUST 1976
2B FLARE
1B
FLARE
NON-FLARE
CONDITIONS
QUIET SUN
LARGE BURST
3B FLARE 8/4/72
WAVELENGTH (nm)
10-7

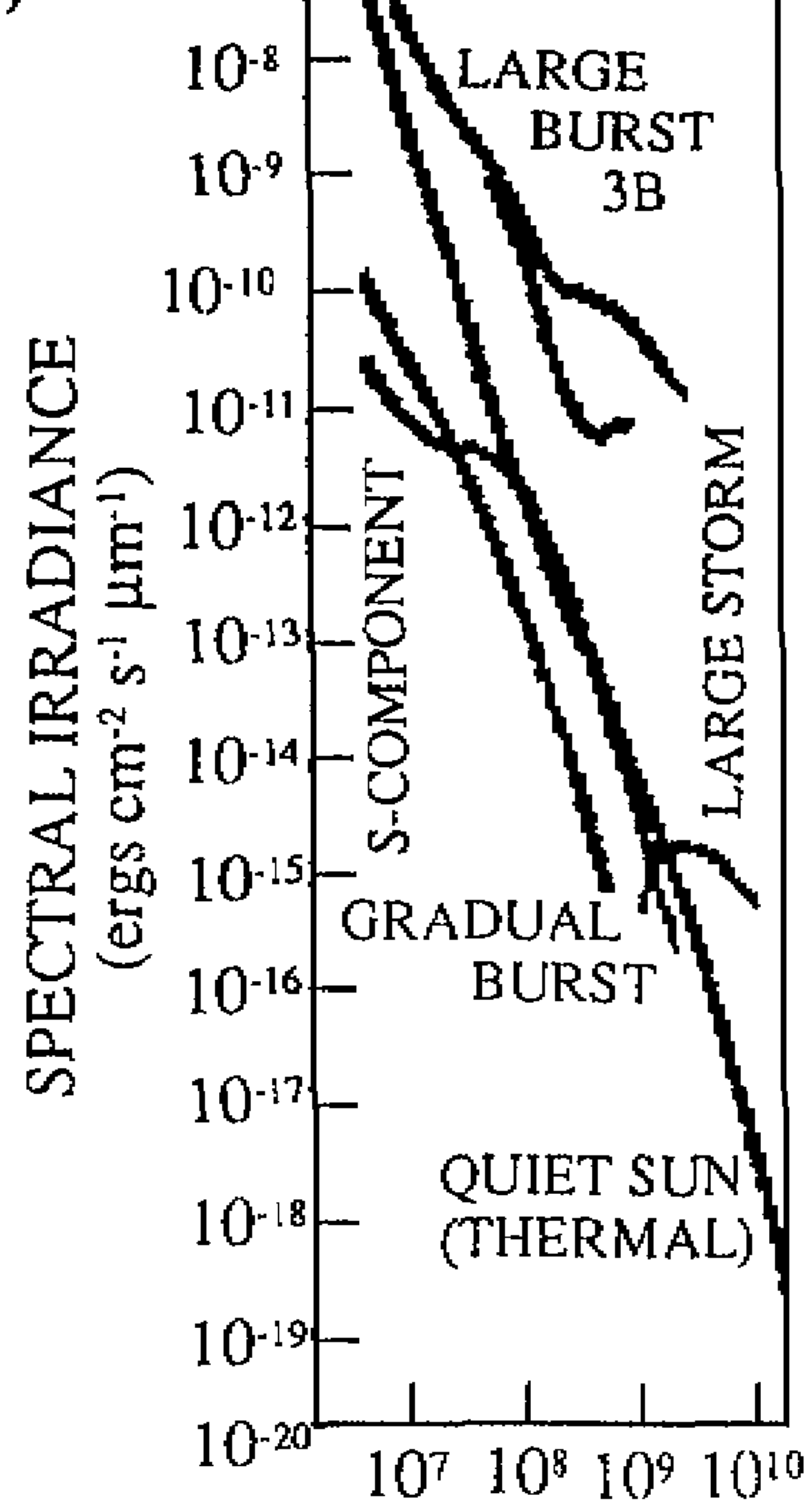

Fig. 3. The solar spectrum from gamma rays to radio wavelengths from *White* [1977].

THE ELECTROMAGNETIC SPECTRUM

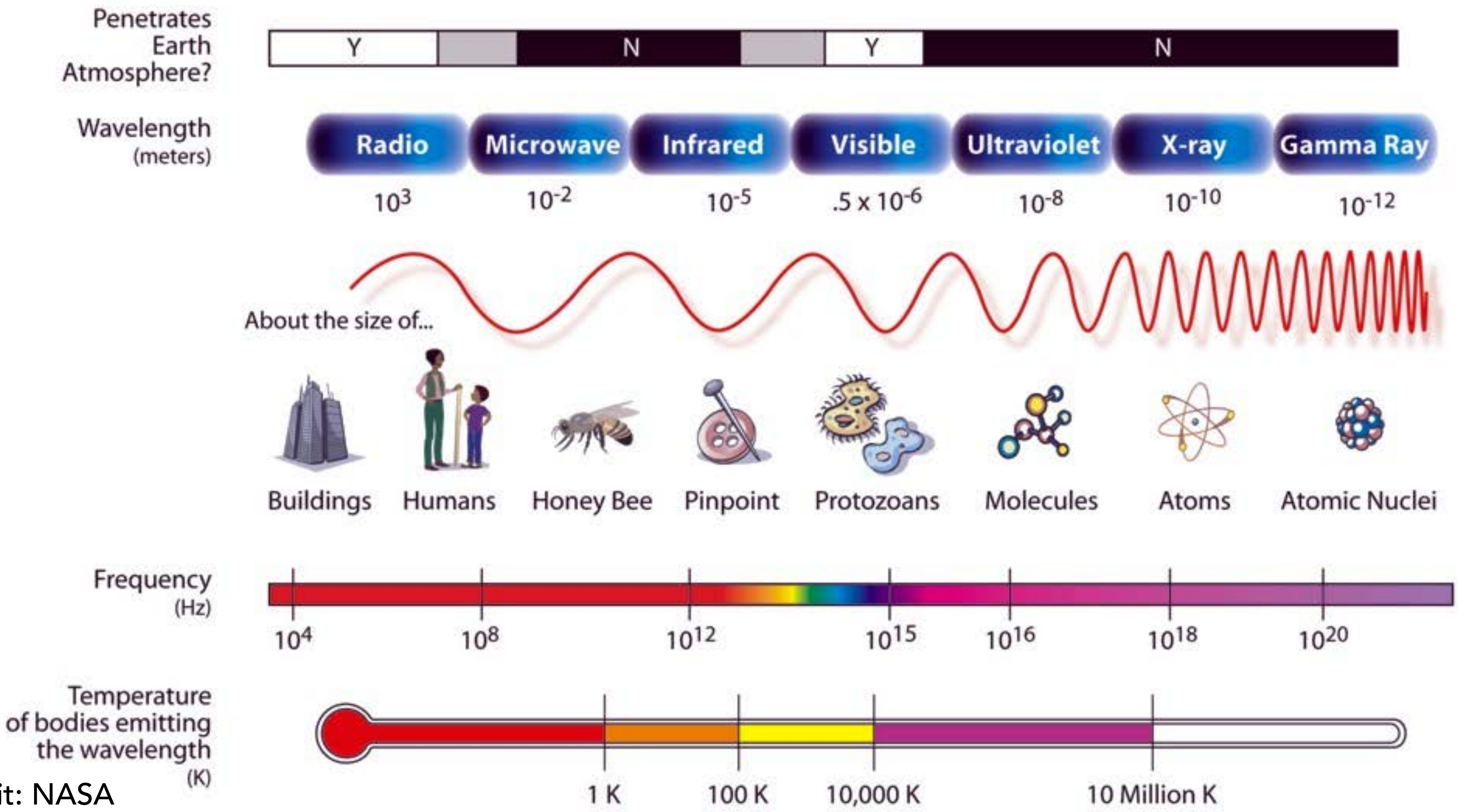

Credit: NASA

Solar Astronomy 101

Most Salient Observational Features about the Sun

- It rotates, but not as a solid body. The equator rotates faster than the poles (use helioseismology to probe the interior).
- It has sunspots. The number of sunspots waxes and wanes with an eleven year cycle.
- Magnetic fields pervade the entire Sun.
- The Sun is a panchromatic astrophysical object.
- The hot corona consists of loops anchored at/near sunspots.
- Total eclipses are awesome (partial eclipses less so). 😎

Upcoming PUNCH mission measures polarized Thomson-scattered light

Eclipse above Oregon on Aug 21st 2017
Credit: Miroslav Druckmüller, Peter Aniol, Shadia Habbal


Sun...Moon...You!
ANNULAR SOLAR ECLIPSE
OCTOBER 14, 2023
APRIL 8, 2024
TOTAL SOLAR ECLIPSE
AMERICAN
ASTRONOMICAL
SOCIETY
Great
American
Eclipse

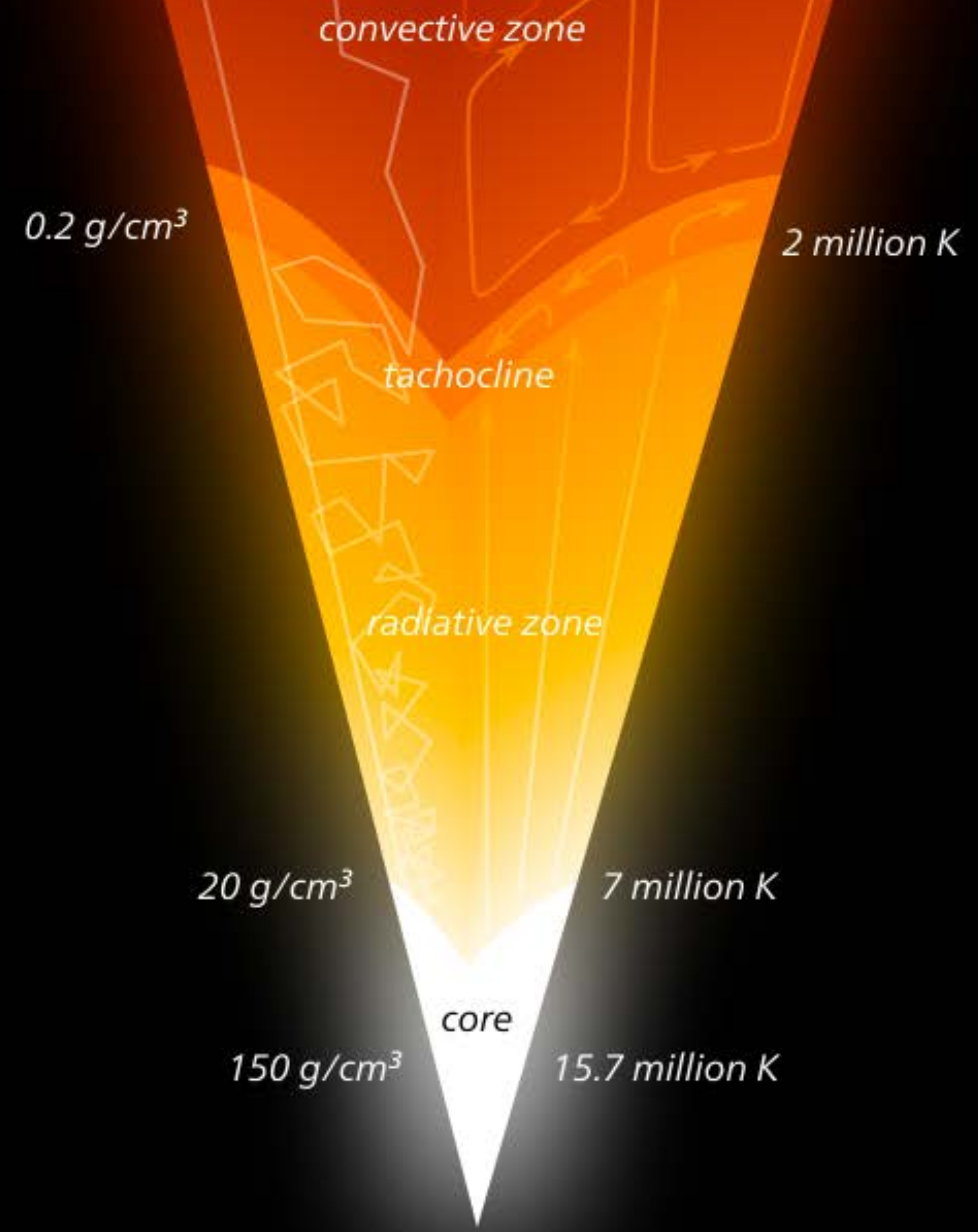

The Solar Interior

Credit: Kelvinsong

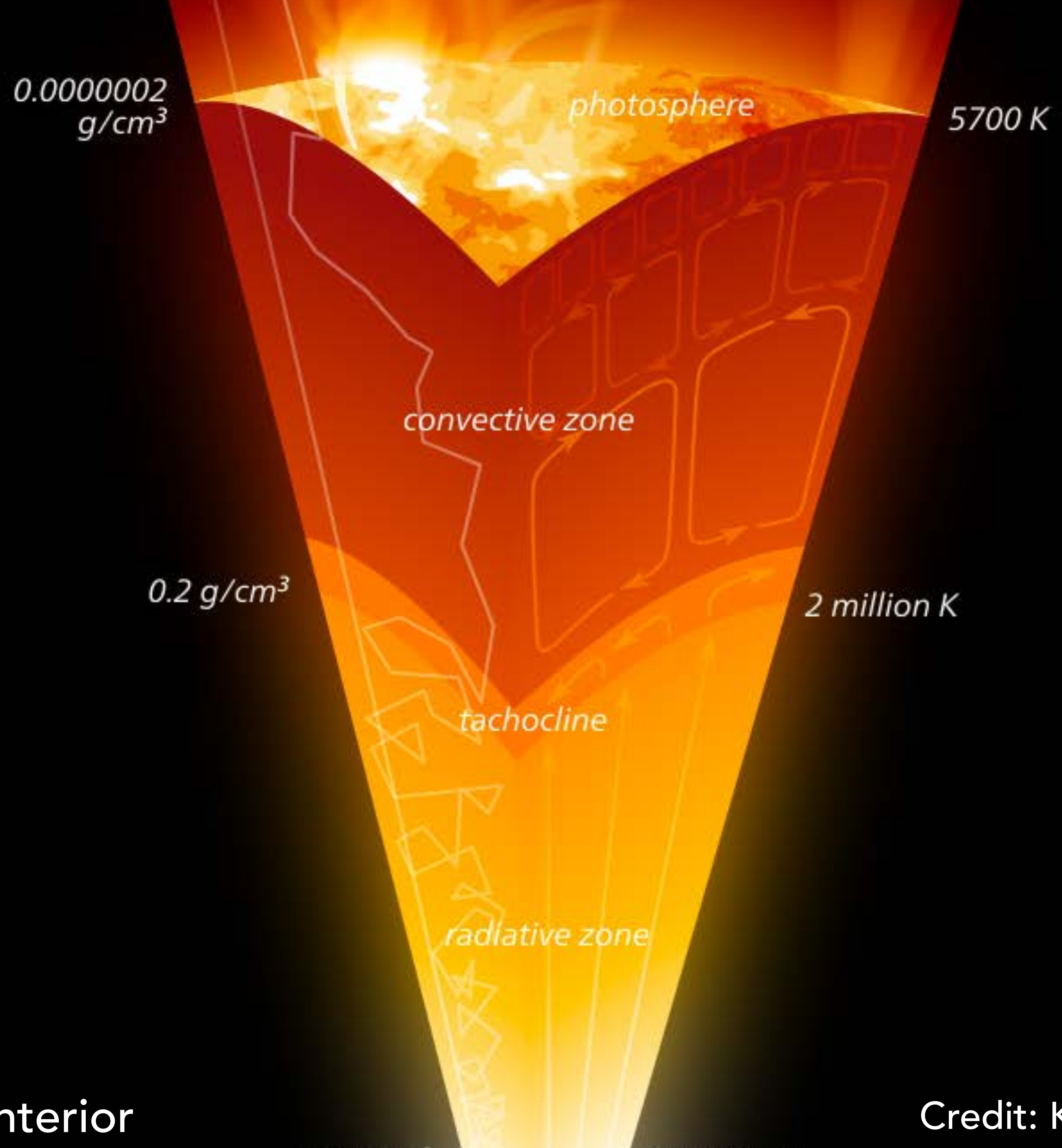

The Solar Interior

Credit: Kelvinsong

Magnetic Field Dominates in the Solar Corona

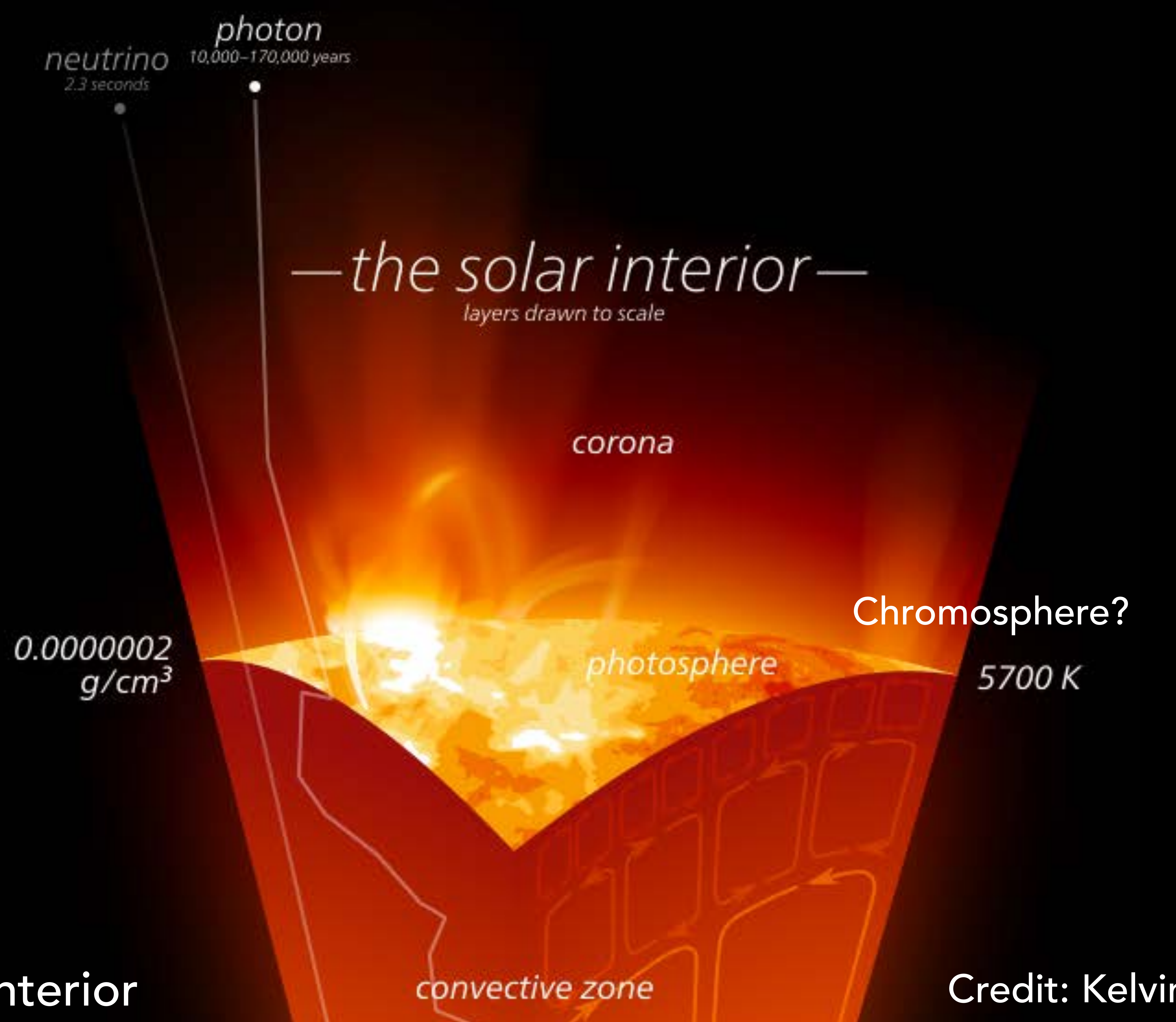

The Solar Interior

Credit: Kelvinsong

Credit: Solar Dynamics Observatory / Stanford

George Ellery Hale

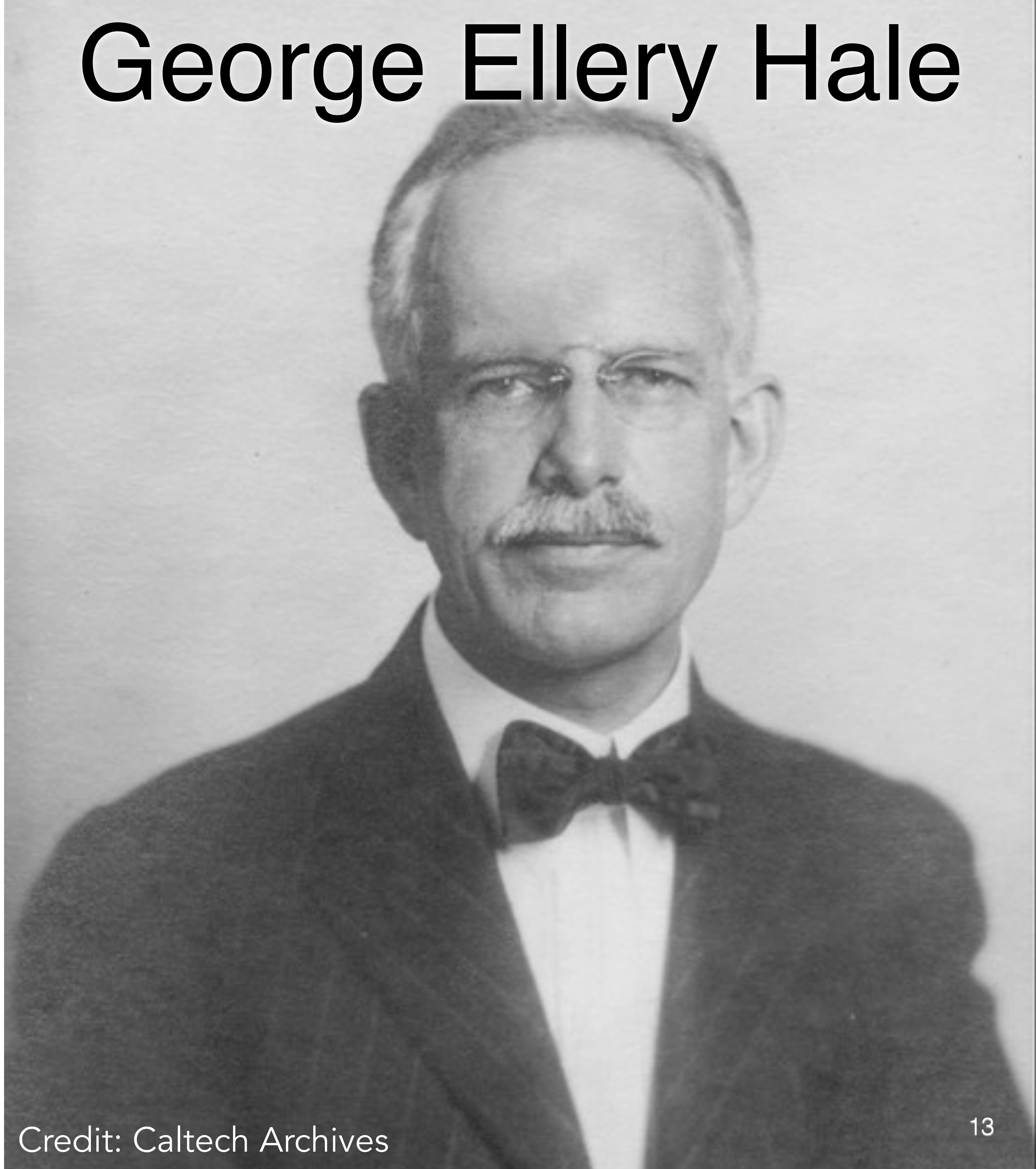

Credit: Caltech Archives

THE MAGNETIC POLARITY OF SUN-SPOTS[1]

BY GEORGE E. HALE, FERDINAND ELLERMAN, S. B. NICHOLSON, AND A. H. JOY

Whirling storms in the earth's atmosphere, whether cyclones or tornadoes, follow a well-known law which is said to have no exceptions: the direction of whirl in the Northern Hemisphere is left-handed or counterclockwise, while in the Southern Hemisphere it is right-handed or clockwise. The theory of terrestrial cyclones is still very obscure, but the direction of whirl is evidently determined by the increase in linear velocity of the air from pole to equator, due to the earth's rotation. The question naturally arises whether storms in the solar atmosphere are also whirlwinds, and, if so, what law governs their direction of whirl in the Northern and Southern hemispheres.

The first definite evidence bearing on this question was obtained with the spectroheliograph in 1908.[2] Photographs of the hydrogen flocculi made with the Hα line showed clearly marked vortical structure in regions centering in sun-spots. This structure was found to be repeated in hundreds of spots, leaving no doubt as to the generality of the phenomenon. Furthermore, photographs were obtained showing masses of hydrogen in the act of being drawn from a great distance toward the center of sun-spots, as though sucked into a vortex.

These photographs suggested the hypothesis that a sun-spot is a vortex, in which electrified particles, produced by ionization in the solar atmosphere, are whirled at high velocity. This might give rise to magnetic fields in sun-spots, regarded as electric vortices. A search for the Zeeman effect led to its immediate detec-

Sunspots are like planet-sized MRI machines

Credit: Swedish Solar Telescope

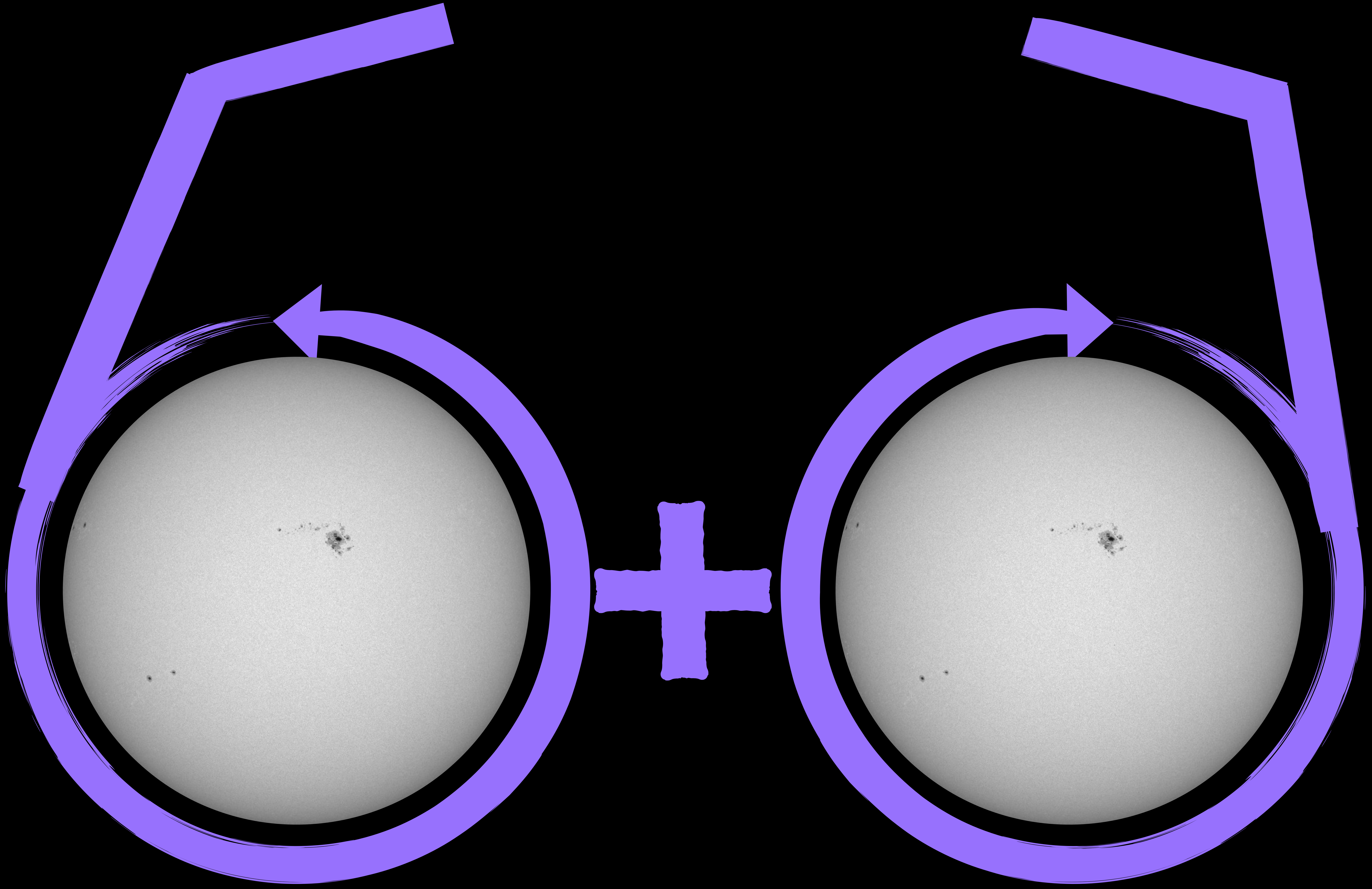

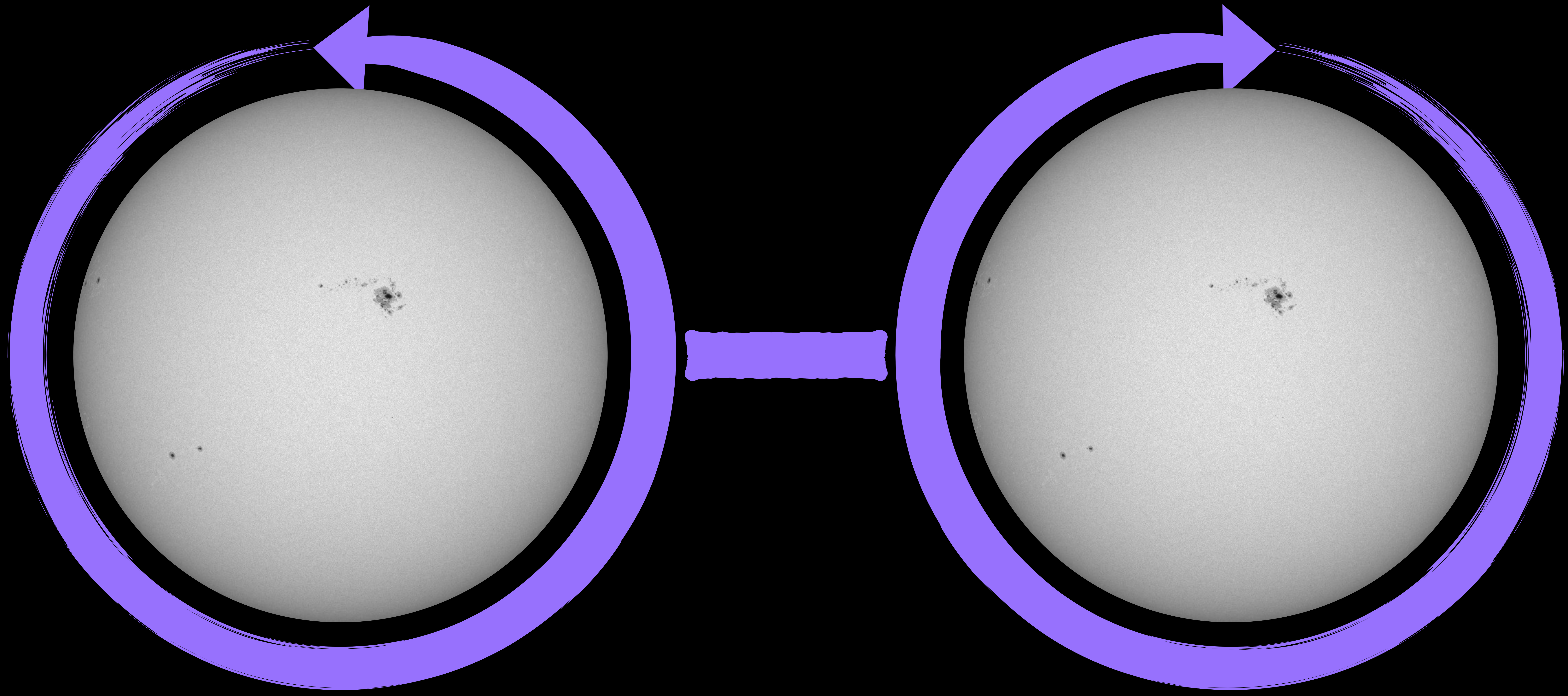

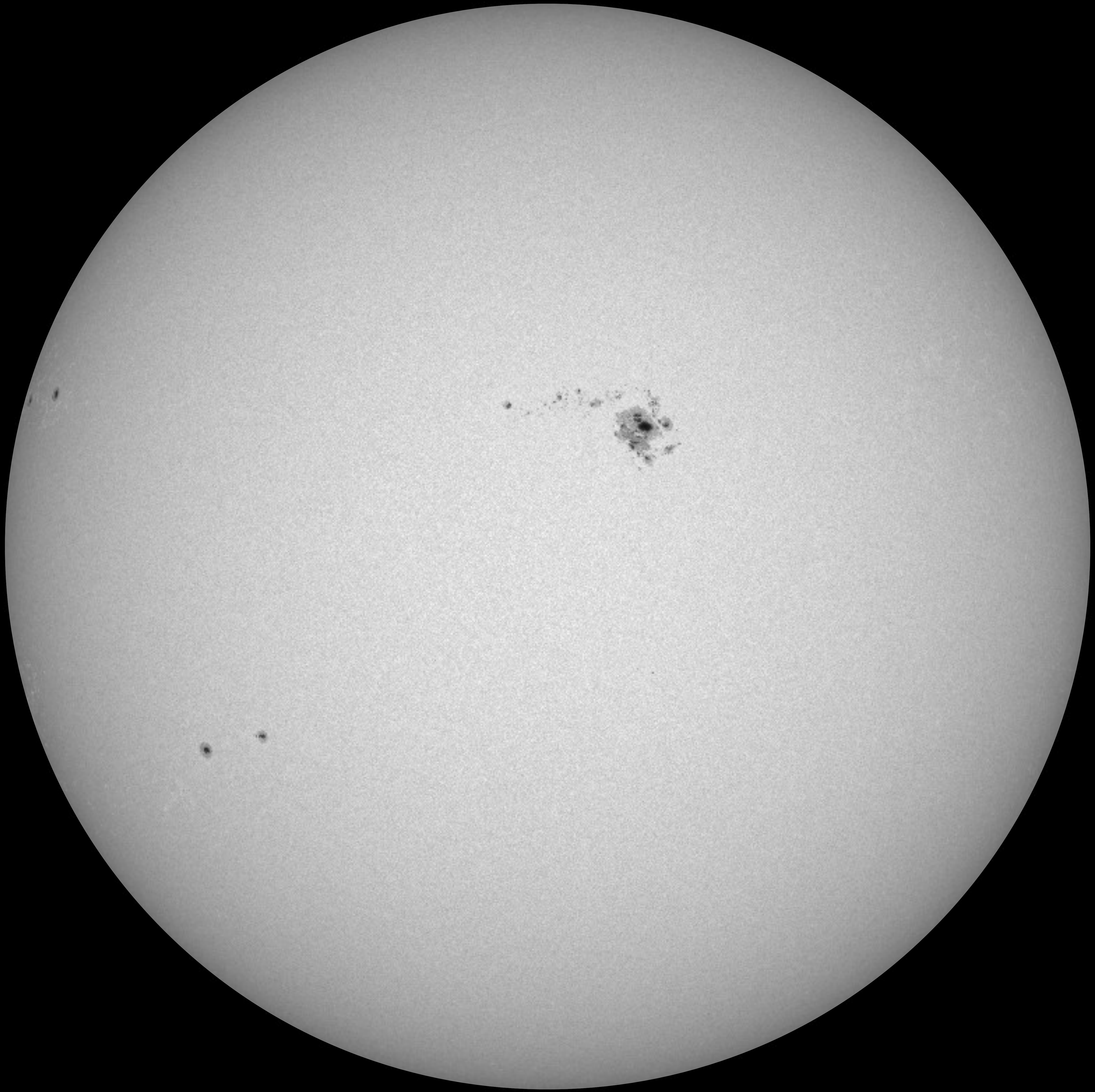

Credit: Solar Dynamics Observatory / Stanford


I
Q
U
V

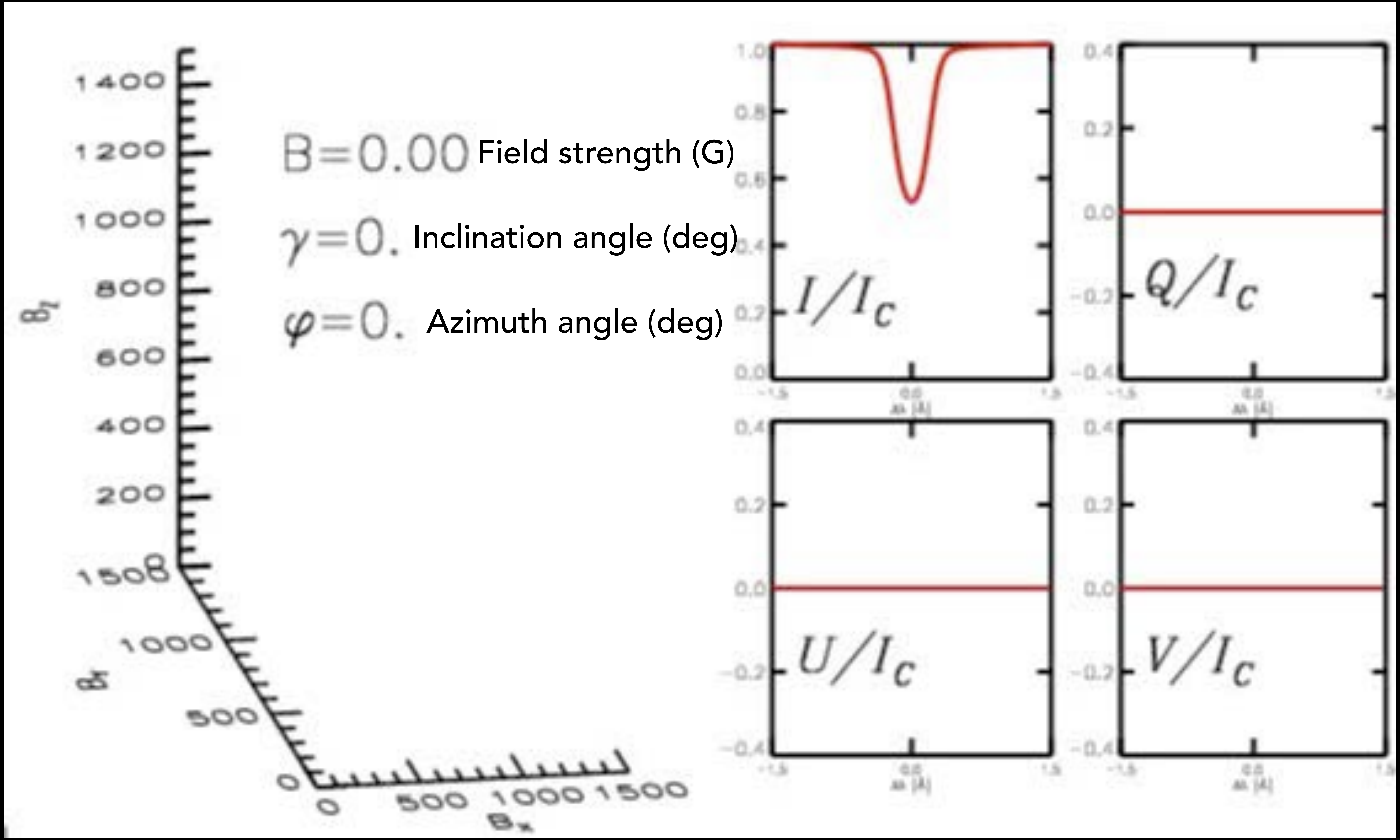

Borrero & Ichimoto (Living Reviews in Solar Physics 2011)

Note: IQUV(φ) = IQUV(φ + 180 deg), known as the 180 deg ambiguity.


NAOJ • LMATC
SOLAR-B
SOT
SOLAR OPTICAL TELESCOPE
JAXA • NASA • MELCO • HAO
https://sot.lmsal.com/Data_new.html
Hinode/Solar Optical Telescope Continuum

https://sot.lmsal.com/Data_new.html

Hinode/Solar Optical Telescope B_{los}

https://sot.lmsal.com/Data_new.html

Hinode/Solar Optical Telescope B_{trans}

HMI vector magnetogram sequence of NOAA AR 11158
Credit: Keiji Hayashi (HMI)

Magnetic Field Dominates in the Solar Corona

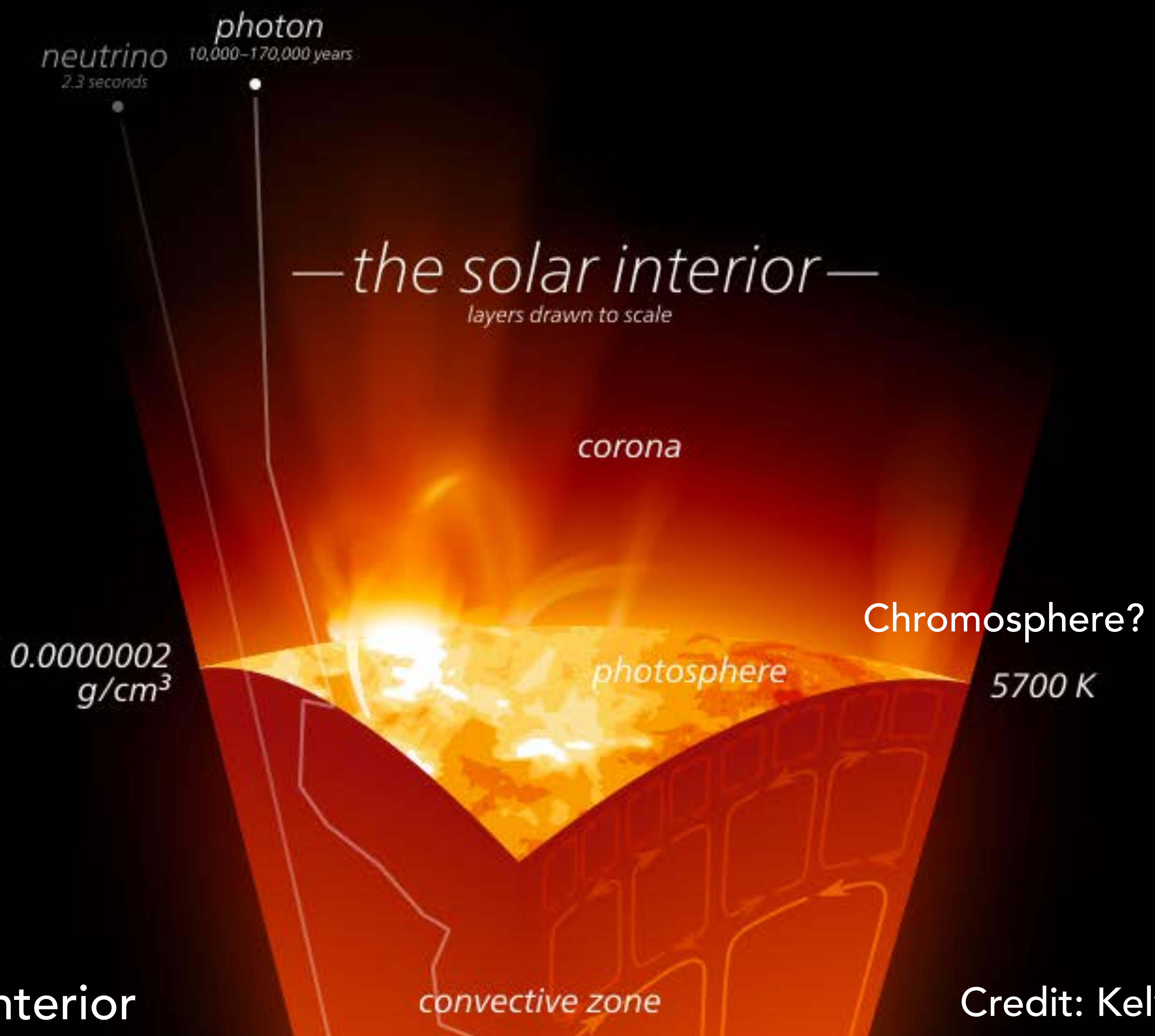

The Solar Interior

Credit: Kelvinsong

Vernazza, Avrett & Loeser (1981)

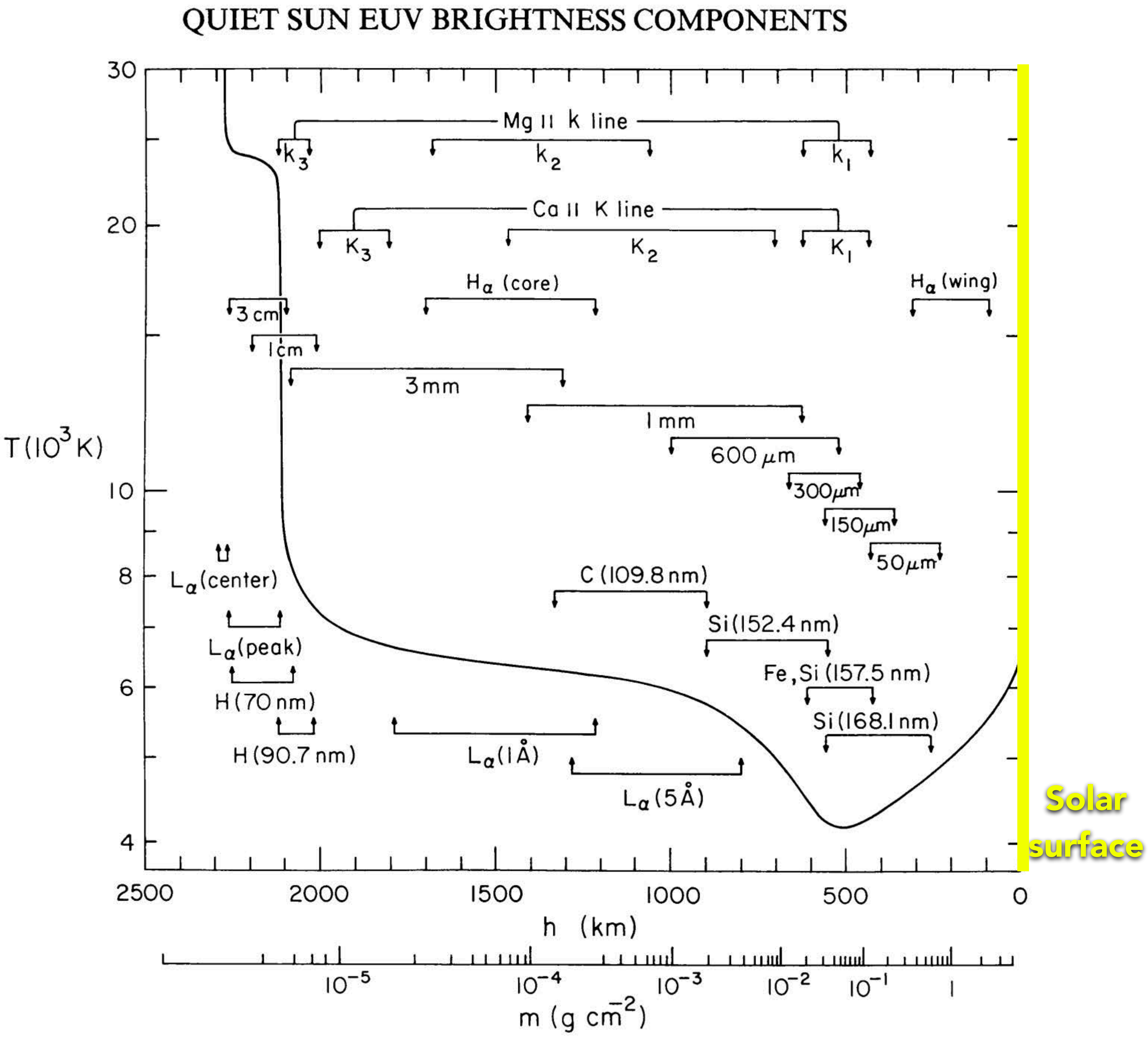

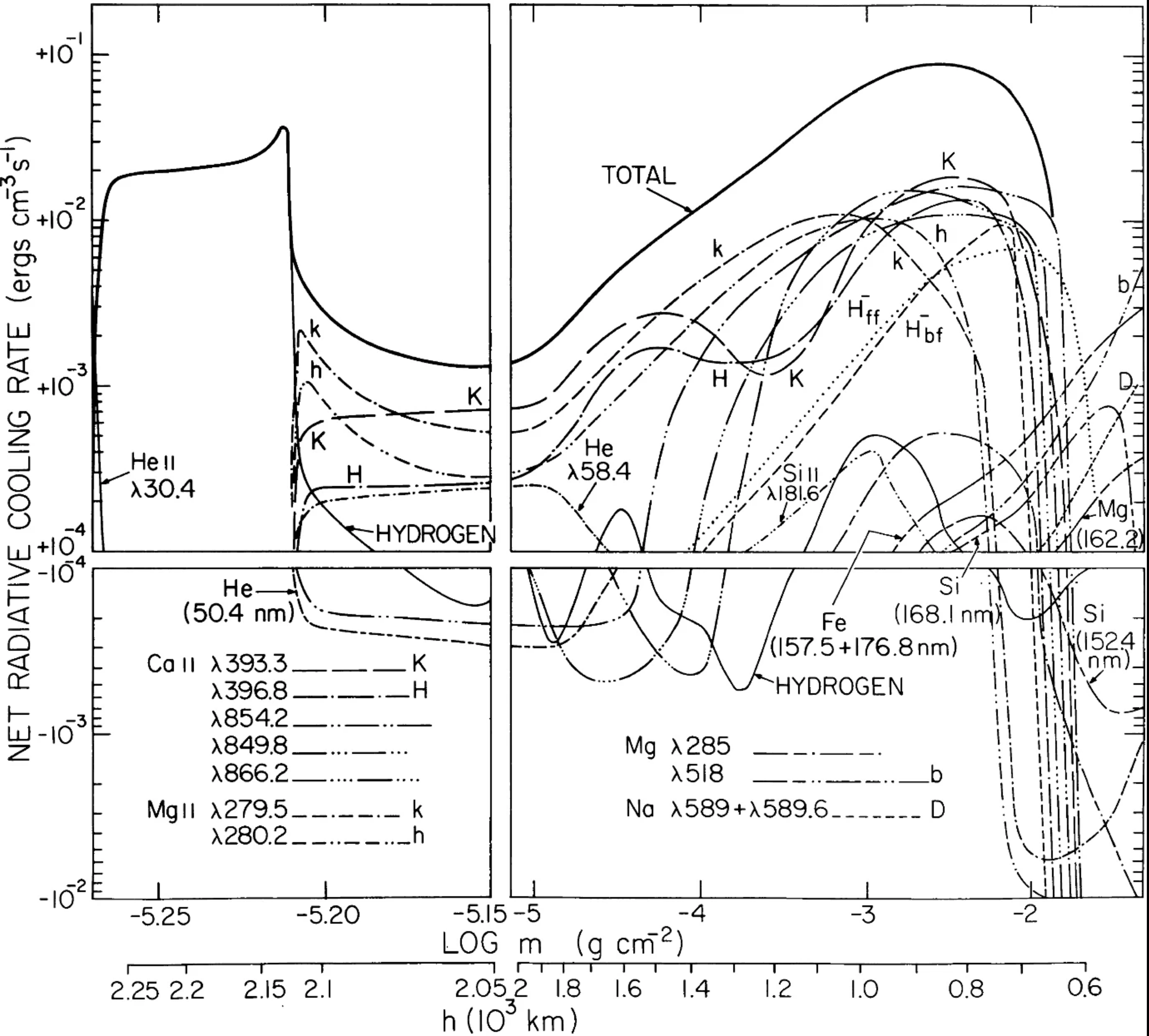

Leenaarts (Living Reviews in Solar Physics, 2020): *"Net radiative cooling in the 1D semi-empirical VAL3C model atmosphere. The cooling between z=700 km and z=2120 km in this model is dominated by five lines from Ca II and two lines from Mg II. At larger heights H I Ly α alone is the dominant radiative cooling agent."*

Wedemeyer-Böhm et al. 2012

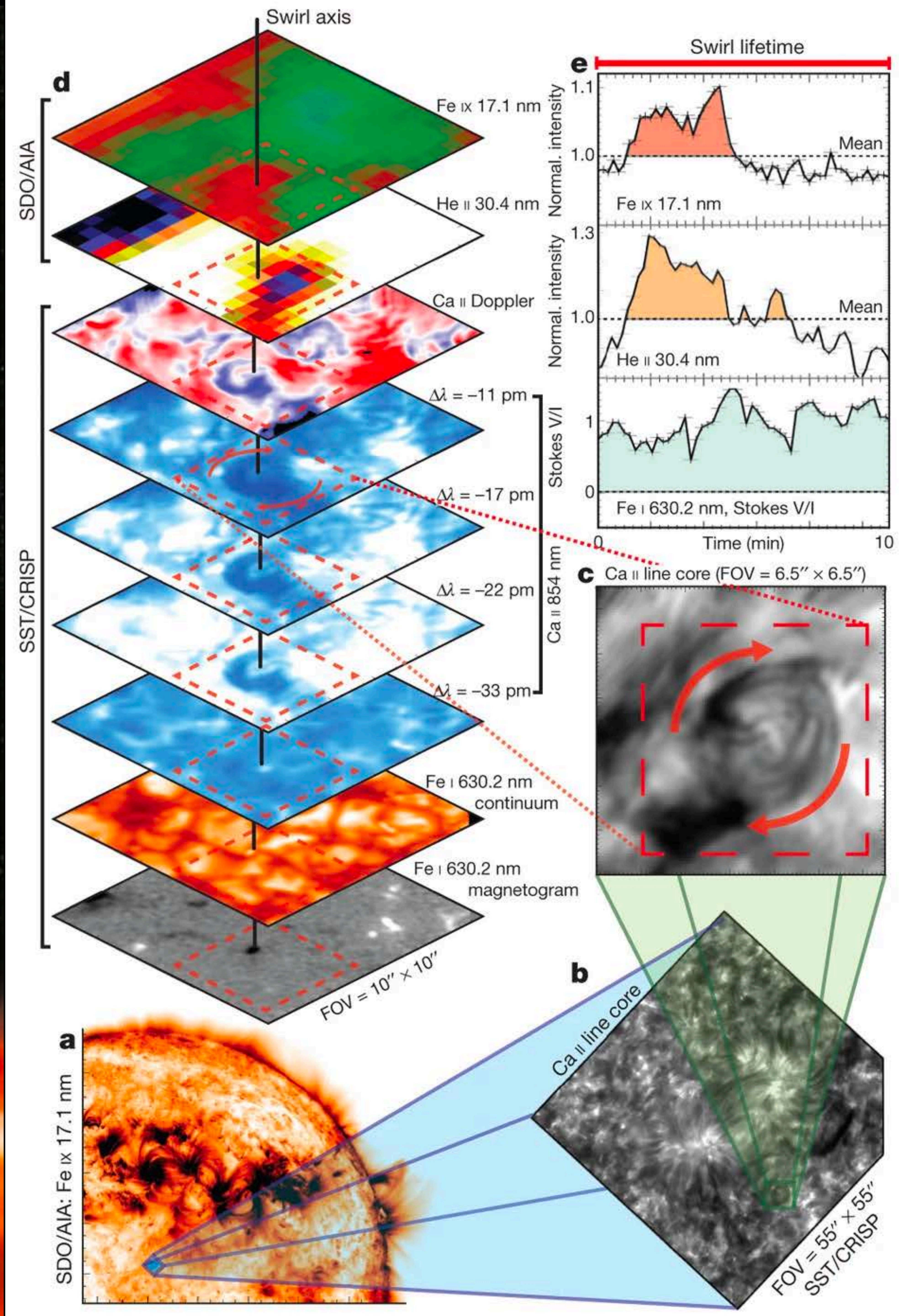

Wedemeyer-Böhm et al. 2009

iris.lmsal.com

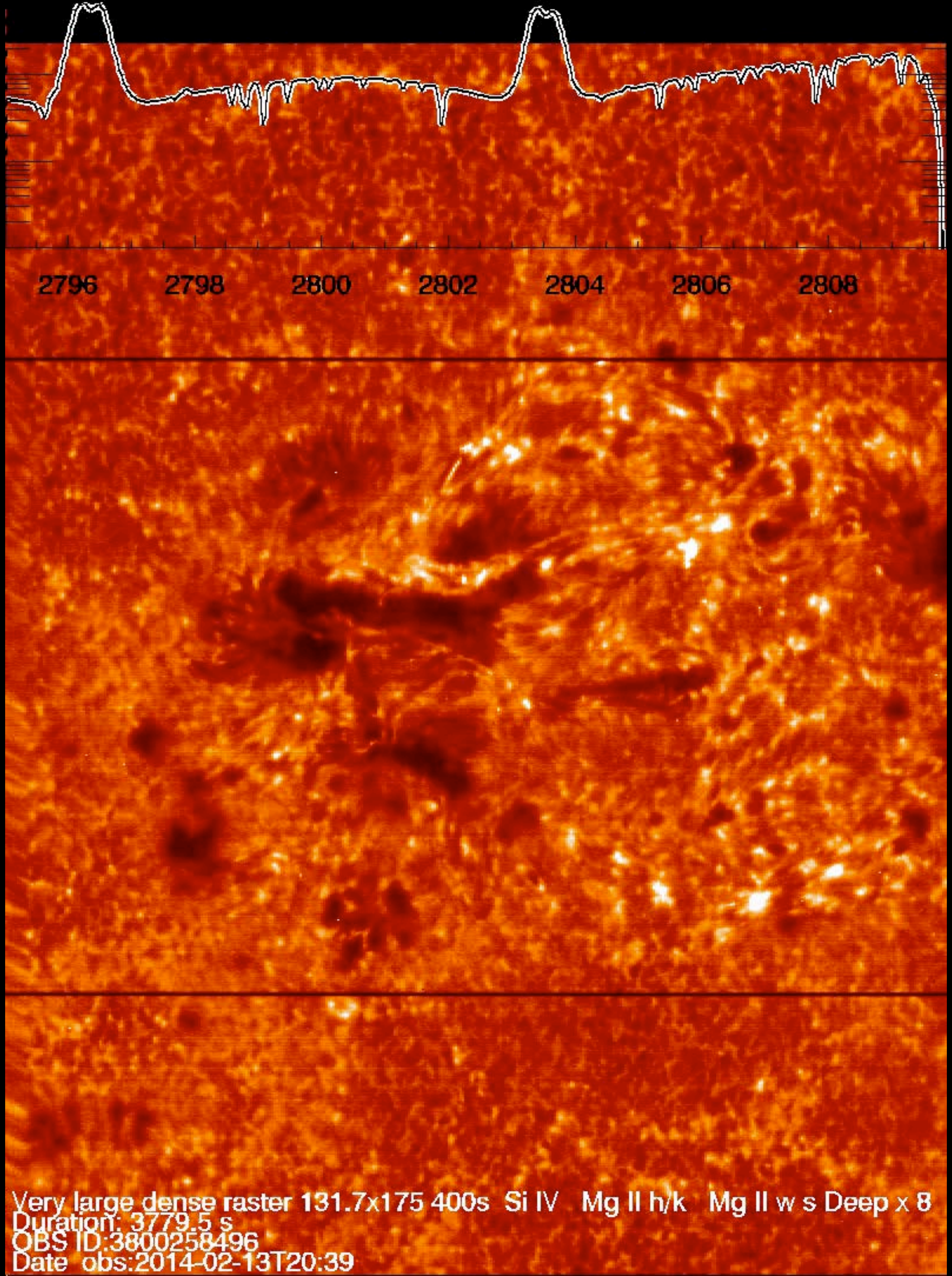

IRIS raster scan of an EFR: Mg II k and Mg II triplet

Scanning from the wing to the k3 (core), one sees the transition from reversed granulation to arch filaments / fibrils.

iris.lmsal.com

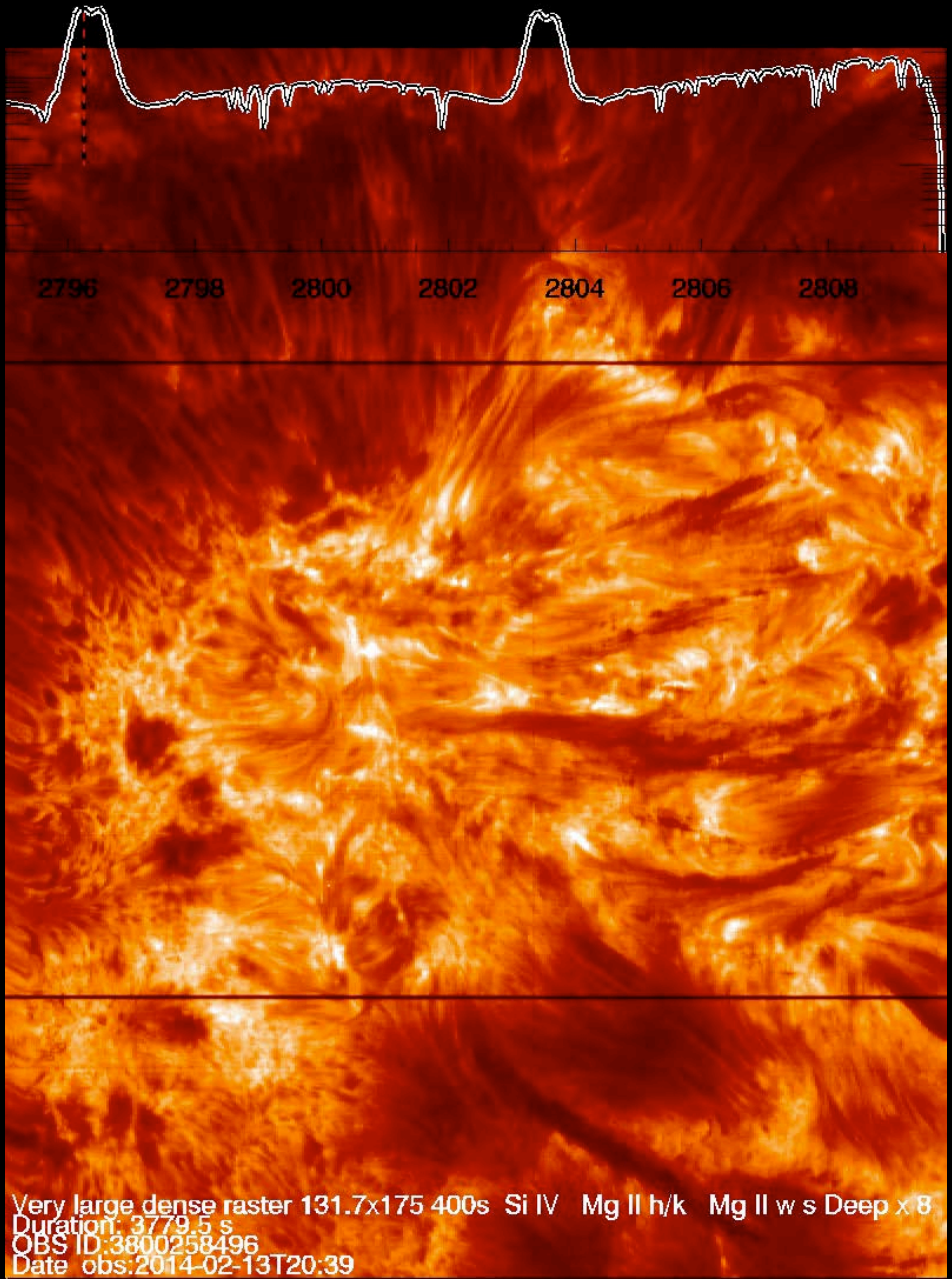

IRIS raster scan of an EFR:
Mg II k and Mg II triplet

Scanning from the wing to the k3 (core), one sees the transition from reversed granulation to arch filaments / fibrils.

iris.lmsal.com

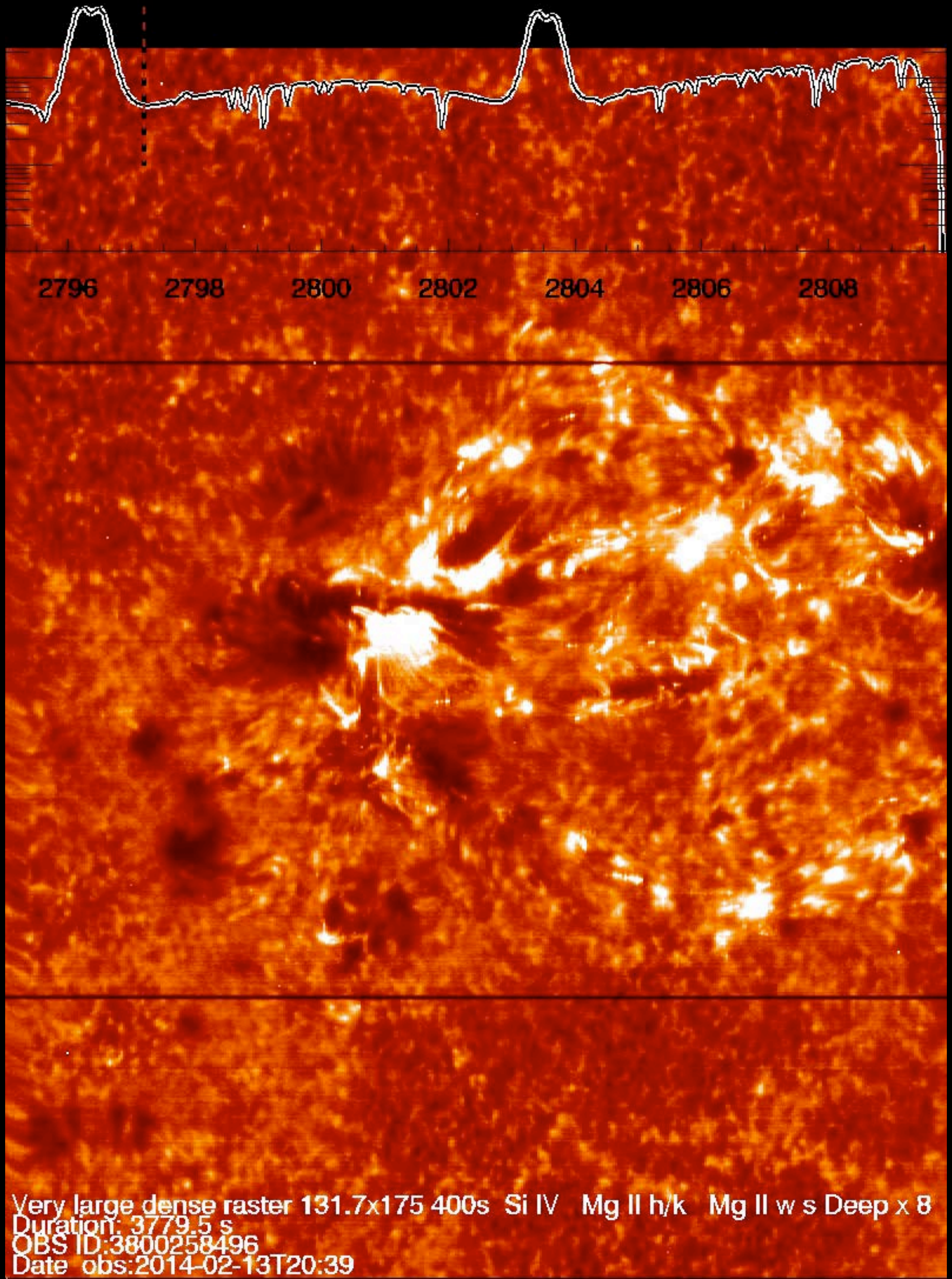

IRIS raster scan of an EFR:
Mg II k and Mg II triplet

Scanning to the Mg II triplet, one sees different structure in the chromosphere (seemingly lower lying loops).

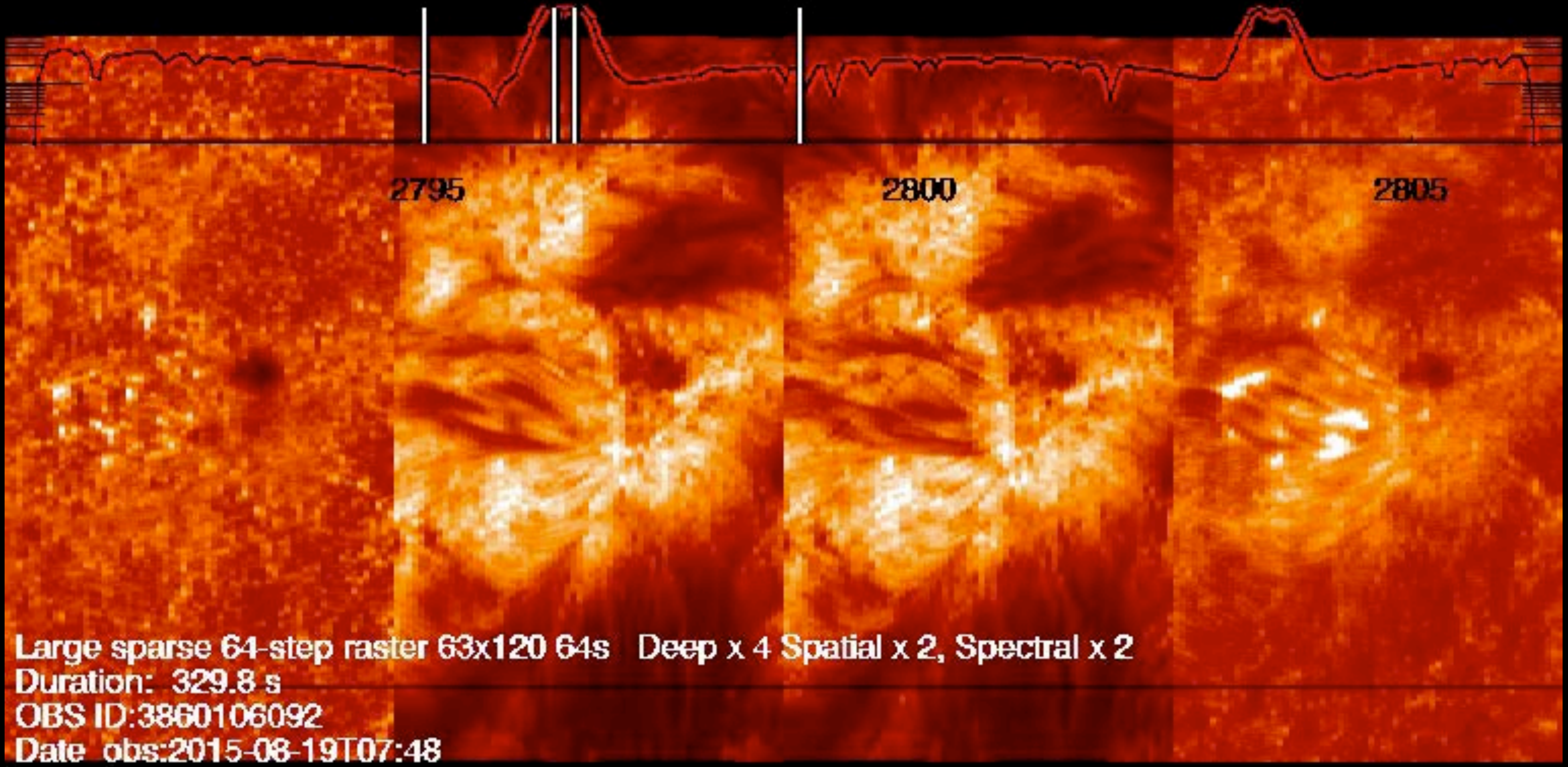

Blue wing Near k2v Near k2r Mg II triplet

IRIS Mg II rasters of an emerging active region @ 330s cadence

Mg II triplet lines are a diagnostics for low chromospheric heating (Pereira et al. 2015)

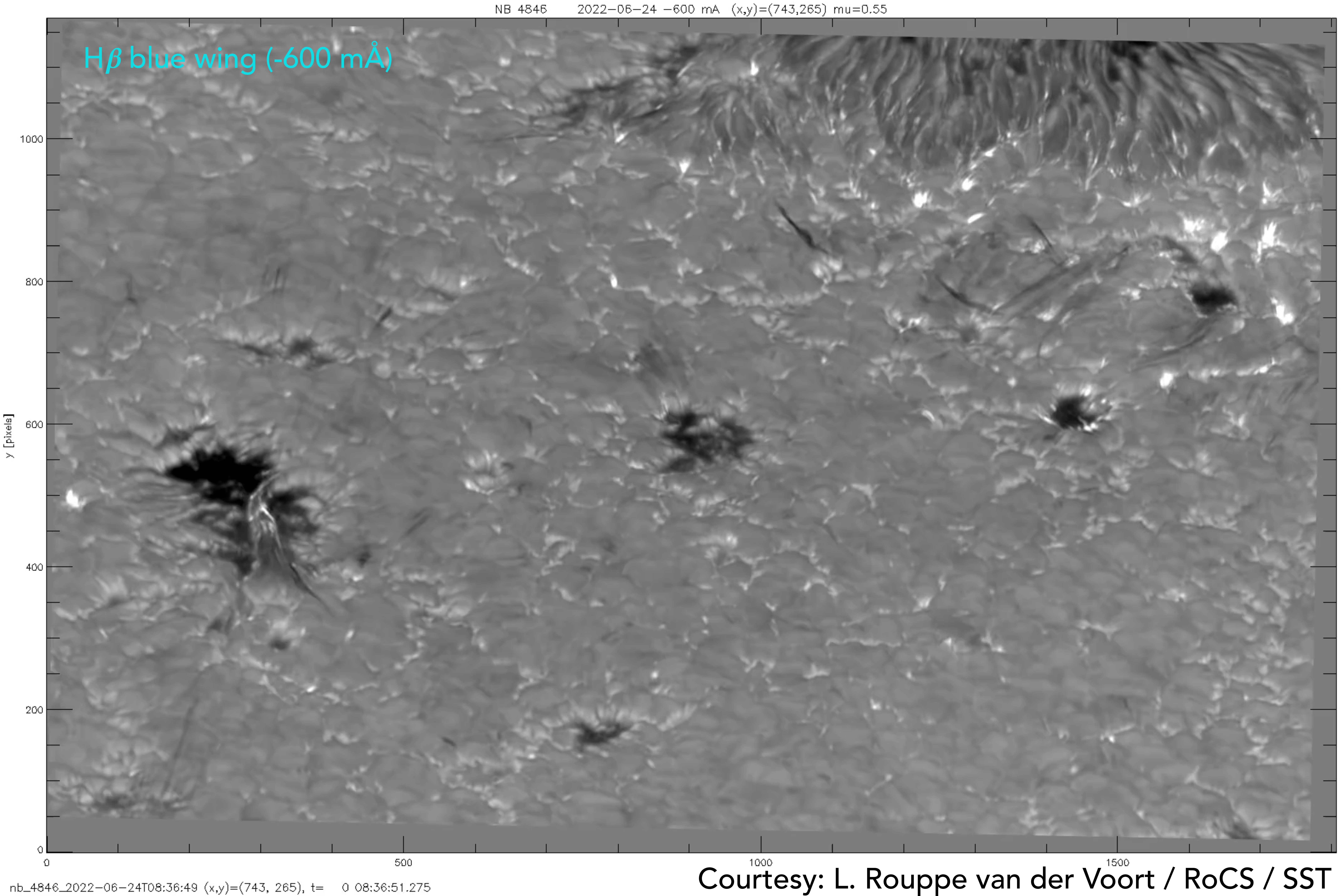

Courtesy: L. Rouppe van der Voort / RoCS / SST

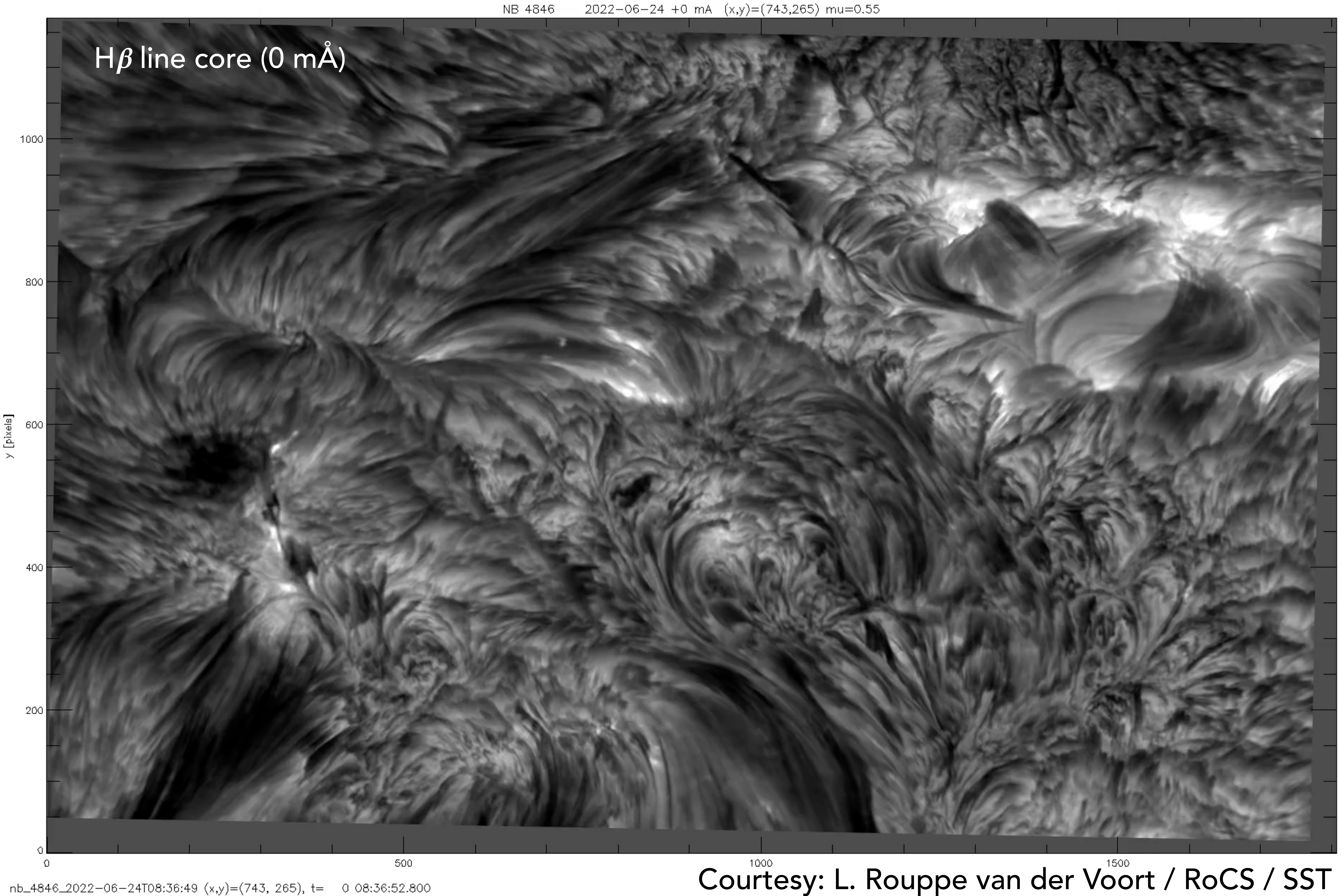
NB 4846 2022-06-24 +0 mA (x,y)=(743,265) mu=0.55
Hβ line core (0 mÅ)
y [pixels]
0
200
400
600
800
1000
0
500
1000
1500
nb_4846_2022-06-24T08:36:49 (x,y)=(743, 265), t= 0 08:36:52.800
Courtesy: L. Rouppe van der Voort / RoCS / SST


Daniel K Inouye Solar Telescope
on Haleakalā, Maui, HI


Courtesy: NSF/NSO/AURA
DKIST VBI red channel ~7058 Å
10,000 km
6,200 miles


Courtesy: NSF/NSO/AURA
DKIST VBI red channel ~7058 Å
12 Dec. 2019
19:24:31 UT

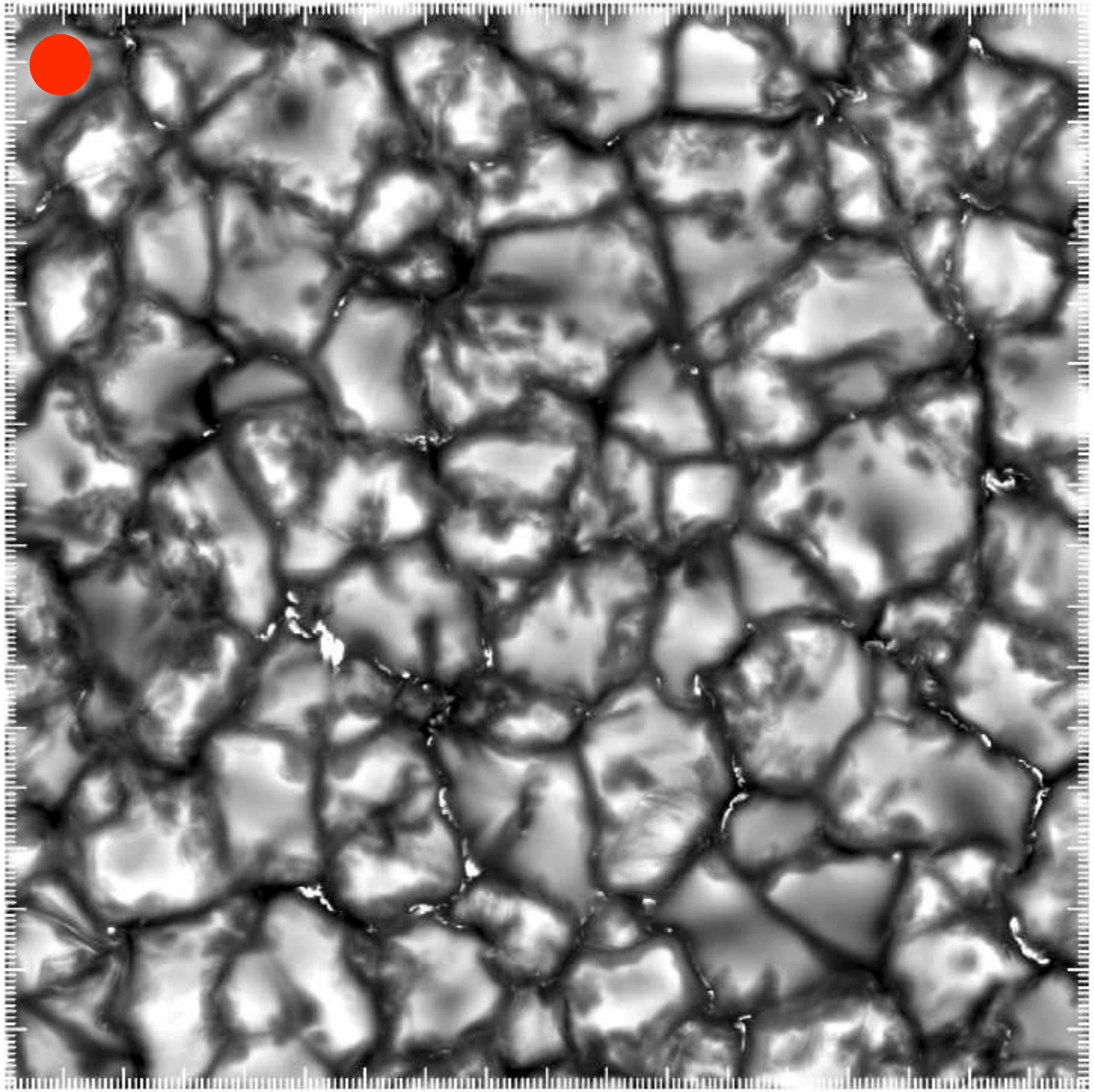

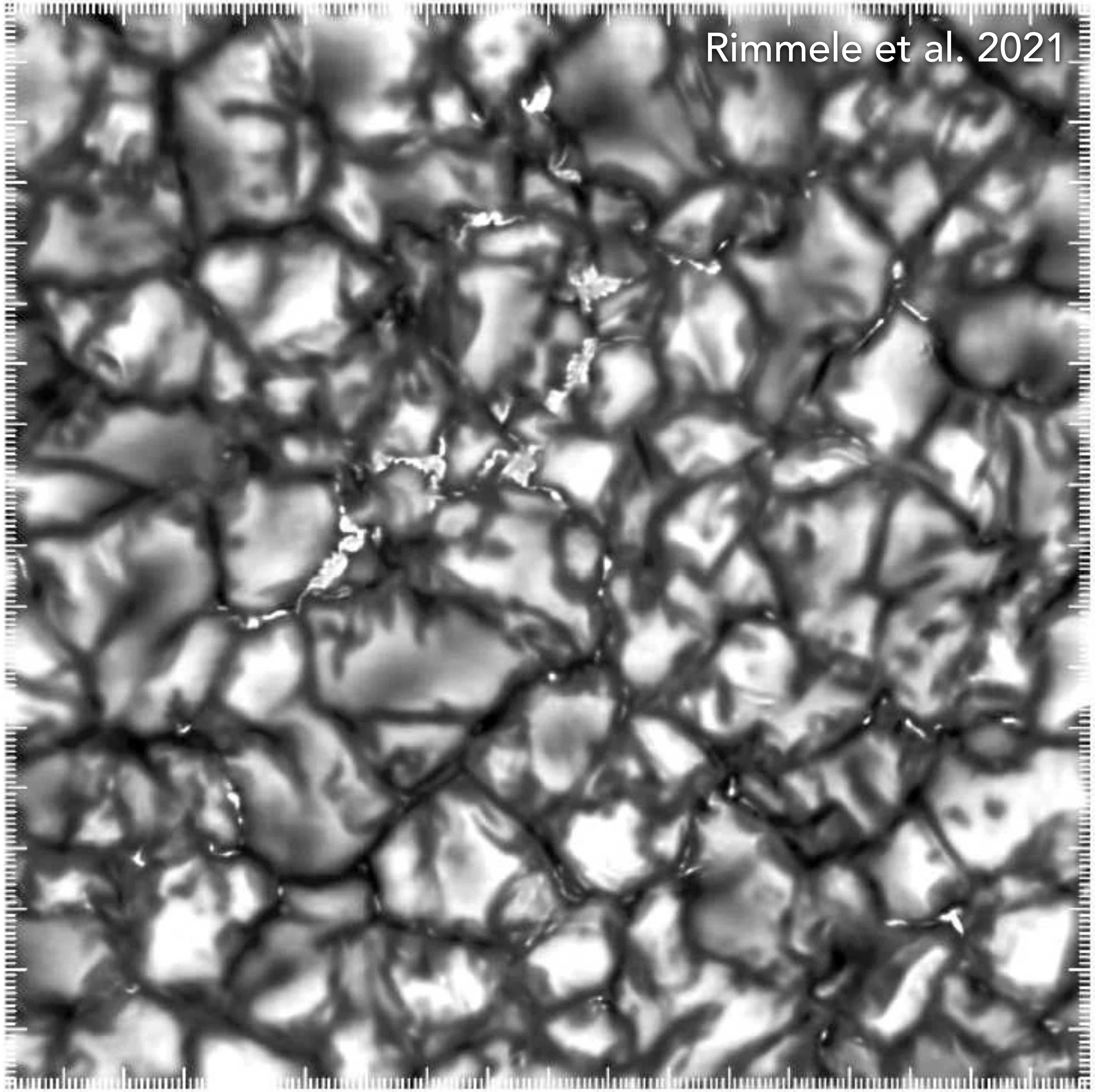

One of these images is a DKIST observation, the other is a synthetic image from a radiative MHD simulation (Rempel 2014). Which is which?

The Coronal Heating Conundrum

- There is lots of energy available.
- The solar atmosphere is strongly stratified.
- Radiative flux at photosphere ~ 6×10^{10} erg cm^{-2} s^{-1}
- Power required to sustain the corona ~ 10^{5-7} erg cm^{-2} s^{-1}
- But that doesn't mean the coronal heating conundrum is uninteresting. Analogy: Food supply in the world.

15 million K	Temperature	1 million K
150 g cm^{-3}	Mass Density	1×10^{-15} g cm^{-3}
2×10^{17} erg cm^{-3}	Internal Energy Density/Pressure	0.1 erg cm^{-3}

SDO images the sun's surface, atmosphere and interior. The mission generates 2 TBs worth of science data everyday.

SDO in a Nutshell

3 instruments monitoring the Sun all the time since May 2010.

- Atmospheric Imaging Assembly: visible, UV, and EUV full disk images of the photosphere, chromosphere, transition region and corona at 4096x4096 pixels.
- Helioseismic & Magnetic Imager: visible light full disk dopplergrams and magnetograms at 4096x4096 pixels.
- EUV Variability Experiment: disk-integrated EUV irradiance spectra at 1 Å resolution.

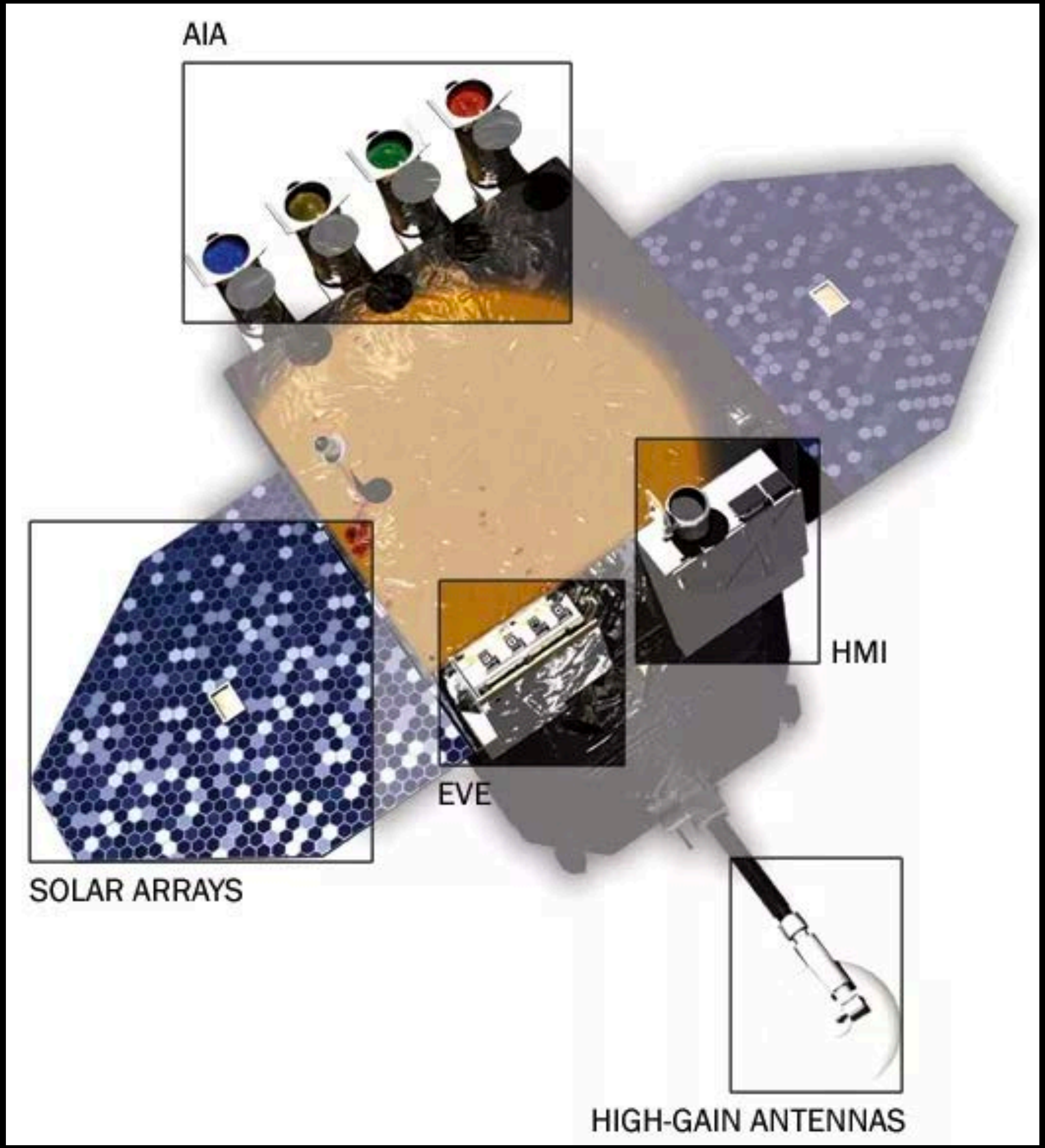

Coronal mass ejection (CME) and flare in SDO/AIA

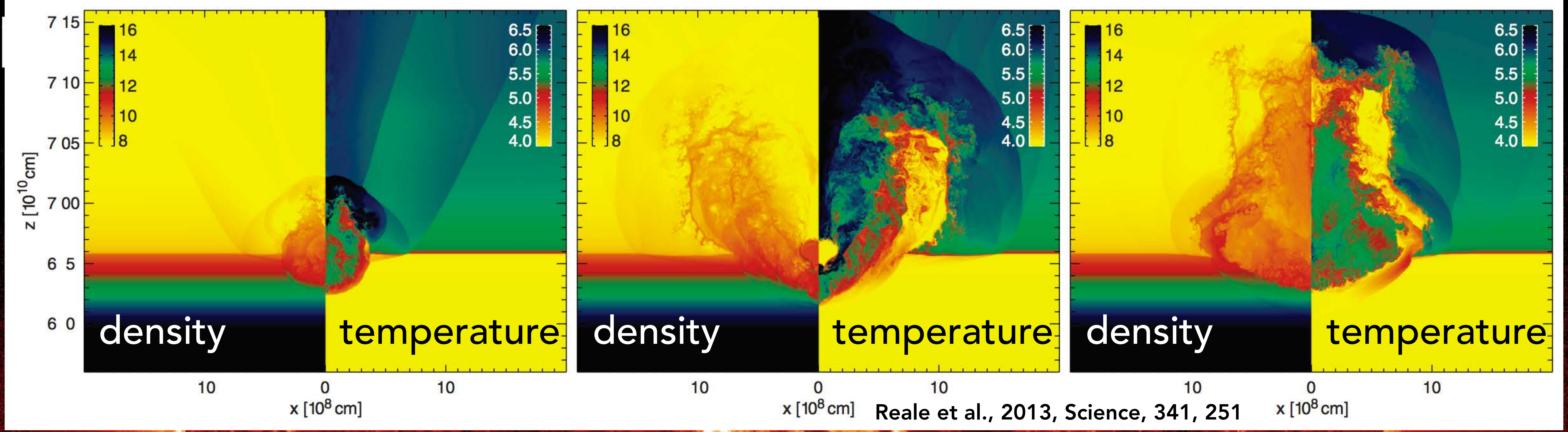

Reale et al., 2013, Science, 341, 251

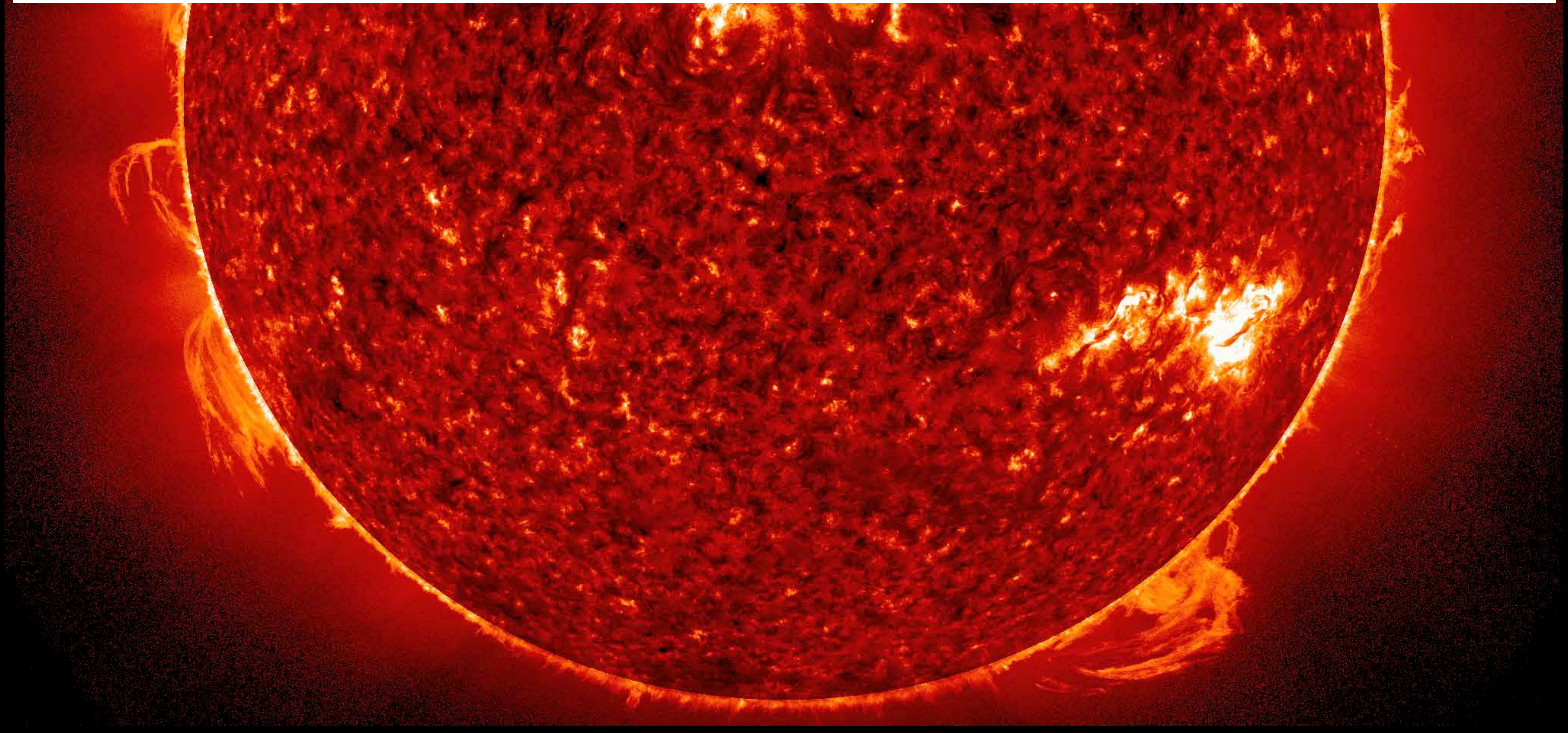

http://svs.gsfc.nasa.gov/4008

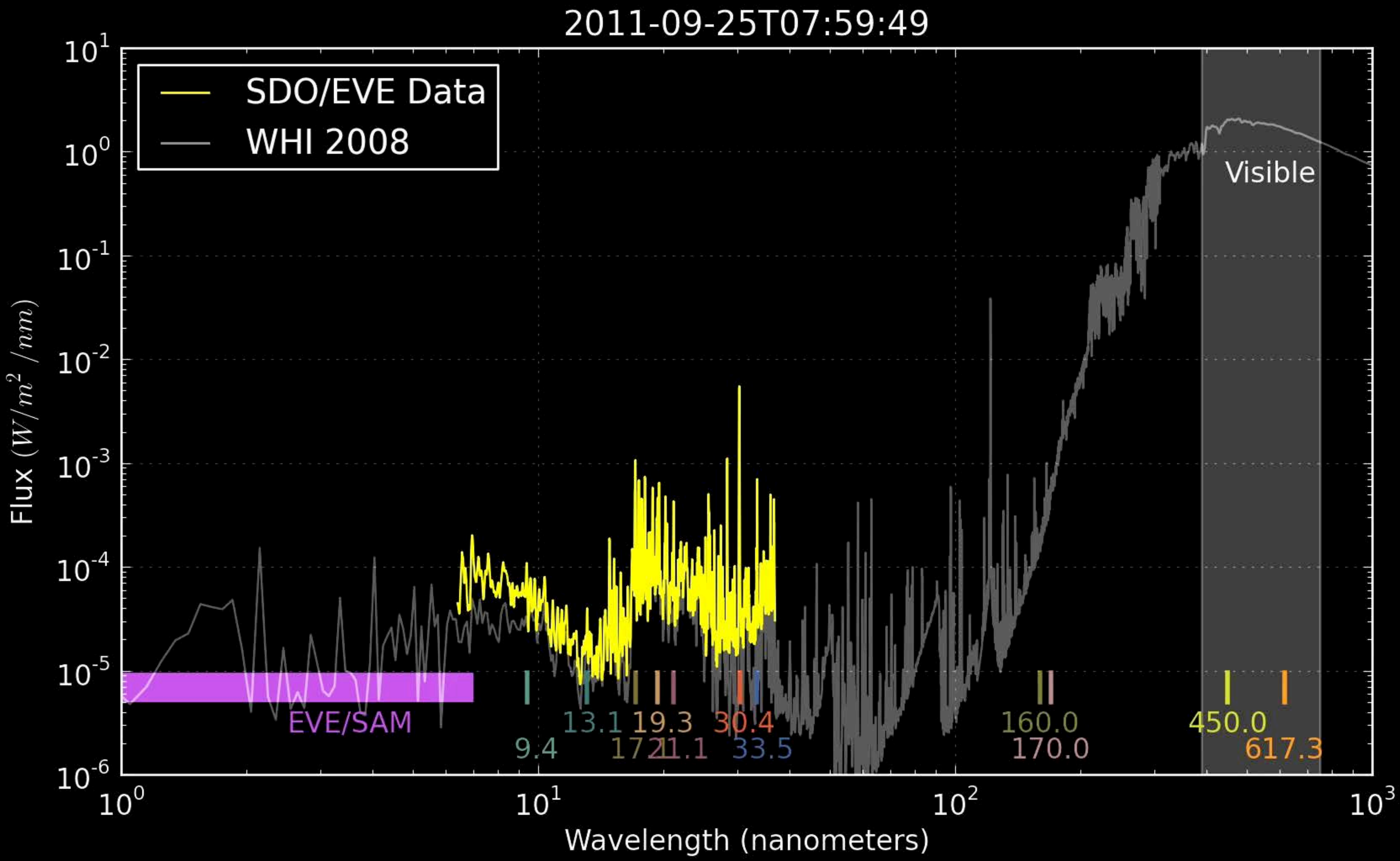

2011-09-25T07:59:49
SDO/EVE Data
WHI 2008
Visible
EVE/SAM
9.4
13.1
172
19.3
21.1
30.4
33.5
160.0
170.0
450.0
617.3
Flux $(W/m^2/nm)$
Wavelength (nanometers)
10^1
10^0
10^{-1}
10^{-2}
10^{-3}
10^{-4}
10^{-5}
10^{-6}
10^0
10^1
10^2
10^3

Szenicer, Fouhey et al. (Science Advances, 2019)

T. Woods

Woods et al. 2011 (ApJ) on late phase flares: "there is typically 40% more energy from this type of flare when including its EUV late phase contribution. "

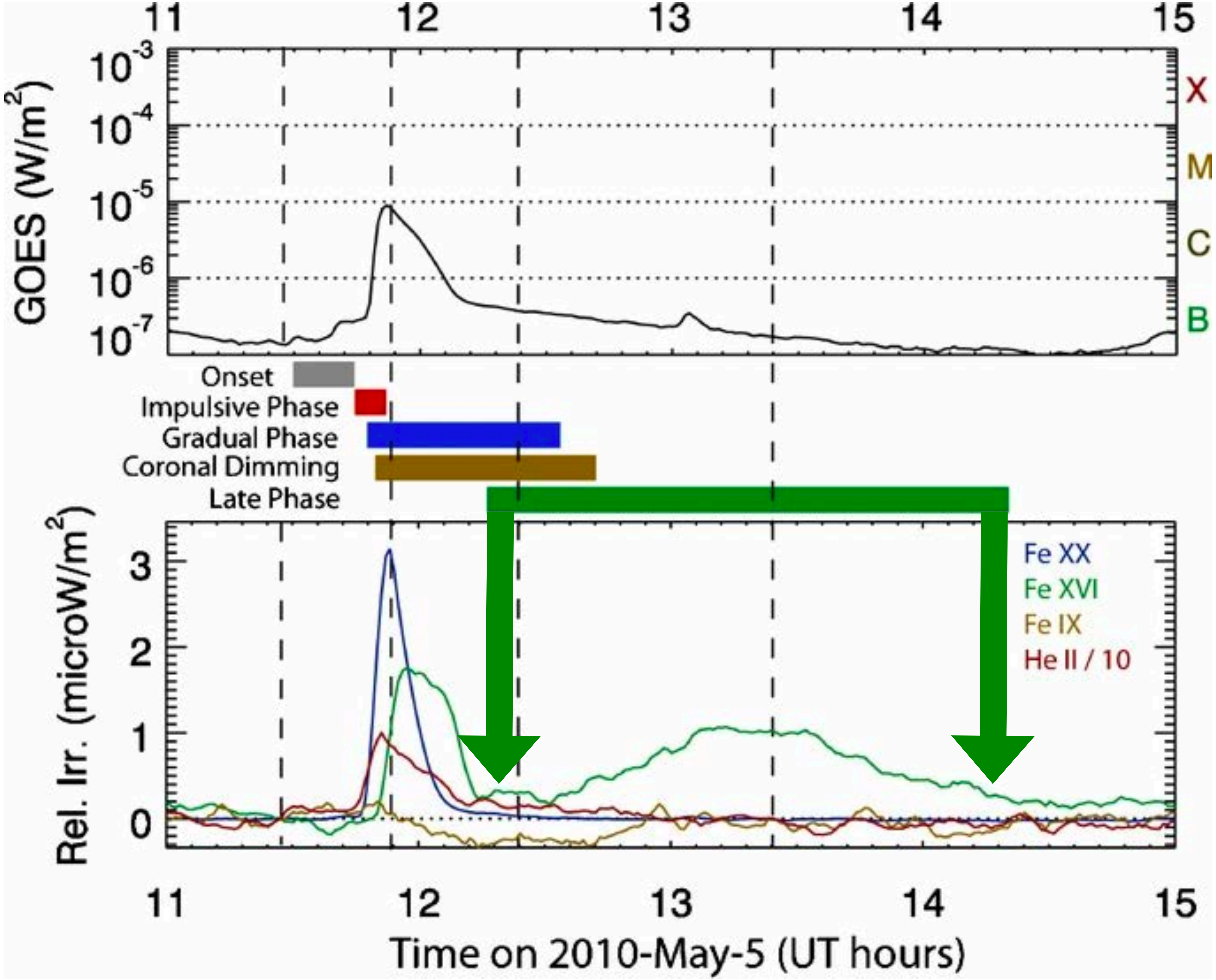

https://lasp.colorado.edu/eve/data_access/index.html

4096x4096 pixel images from SDO's Atmospheric Imaging Assembly (AIA) instrument

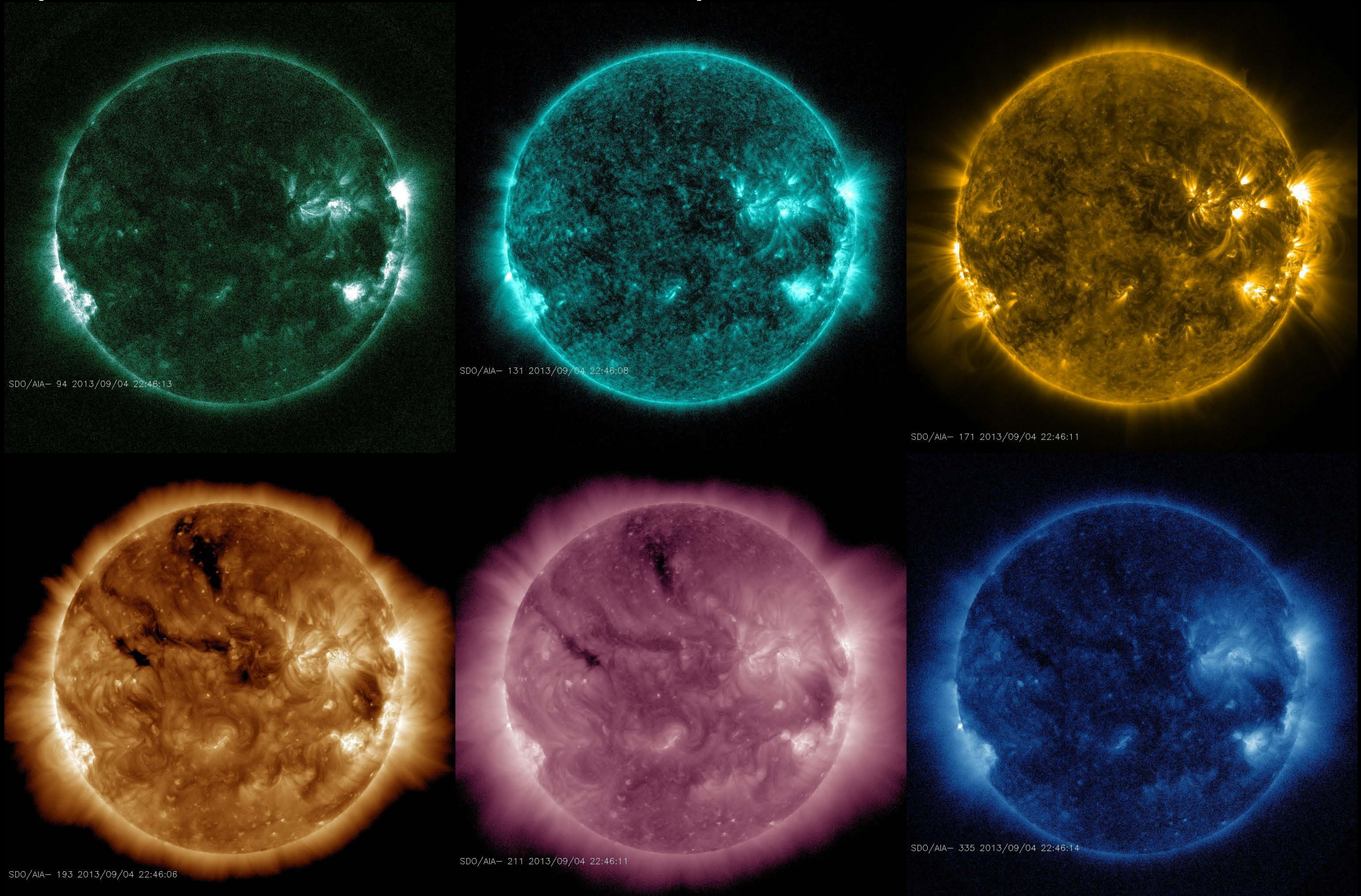

Retrieval of temperature "Emission Measure" (EM) maps is an compressed sensing problem.

AIA Temperature Response Functions

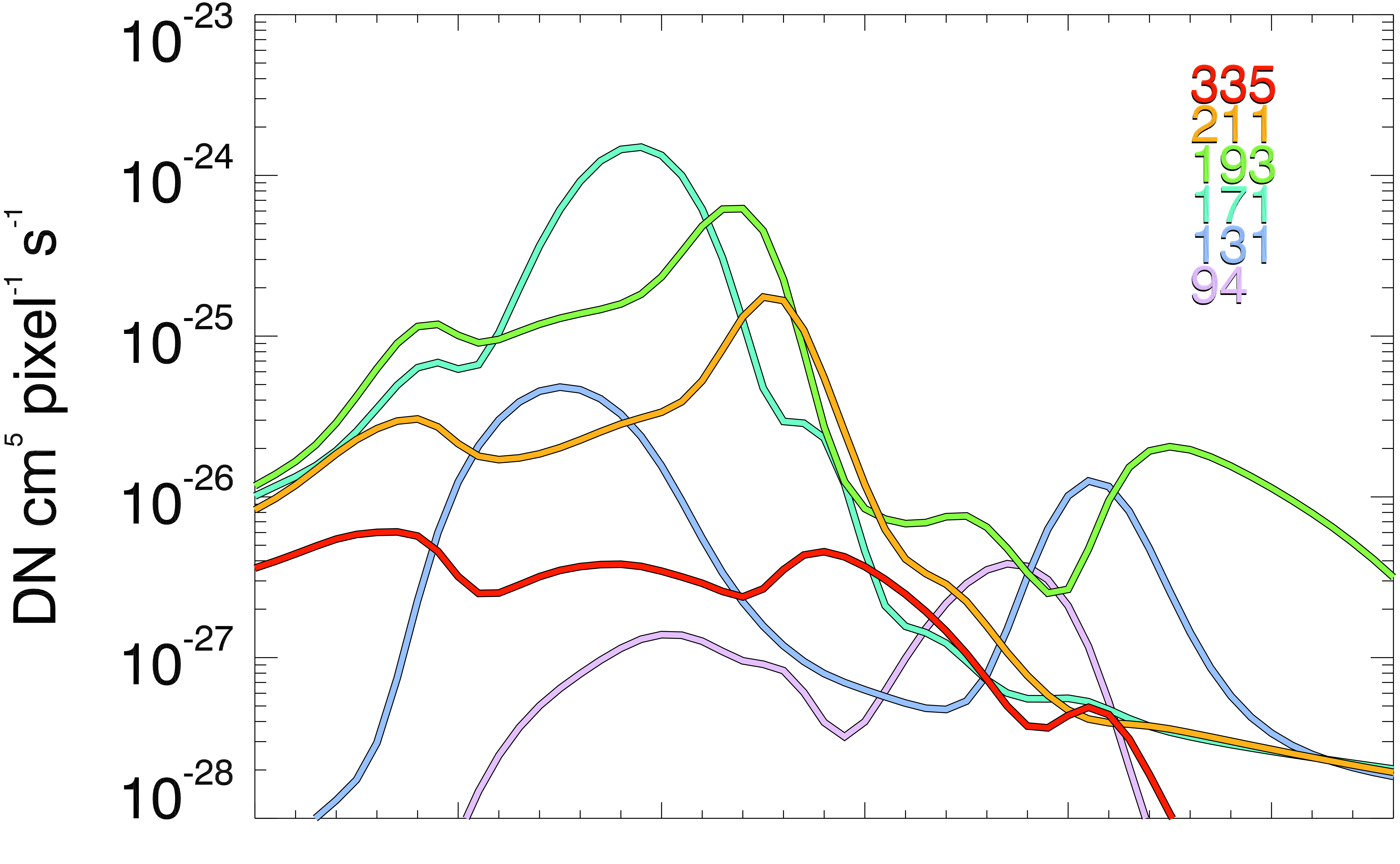

Cheung et al.
(Astrophysical Journal, 2015)

Problem Statement

$\boldsymbol{x} = \boldsymbol{Km} = \boldsymbol{KDy}$

rows of $\boldsymbol{K}$ = response of wavelength channel

$\boldsymbol{x}$ = detector counts

$\boldsymbol{m} = \boldsymbol{Dy}$,

cols. of $\boldsymbol{D}$ = basis funcs

m = emission measure (EM) in temperature bins

EM = line-of-sight integral of electron density squared

Major EUV Lines in SDO/AIA passbands

Table 1. Predicted AIA count rates.

	Ion	λ Å	T_p^a K	Fraction of total emission CH	QS	AR	FL
94 Å	Mg VIII	94.07	5.9	0.03	-	-	-
	Fe XX	93.78	7.0	-	-	-	0.10
	Fe XVIII	93.93	6.85	-	-	0.74	0.85
	Fe X	94.01	6.05	0.63	0.72	0.05	-
	Fe VIII	93.47	5.6	0.04	-	-	-
	Fe VIII	93.62	5.6	0.05	-	-	-
	Cont.			0.11	0.12	0.17	-
131 Å	O VI	129.87	5.45	0.04	0.05	-	-
	Fe XXIII	132.91	7.15	-	-	-	0.07
	Fe XXI	128.75	7.05	-	-	-	0.83
	Fe VIII	130.94	5.6	0.30	0.25	0.09	-
	Fe VIII	131.24	5.6	0.39	0.33	0.13	-
	Cont.			0.11	0.20	0.54	0.04
171 Å	Ni XIV	171.37	6.35	-	-	0.04	-
	Fe X	174.53	6.05	-	0.03	-	-
	Fe IX	171.07	5.85	0.95	0.92	0.80	0.54
	Cont.			-	-	-	0.23
193 Å	O V	192.90	5.35	0.03	-	-	-
	Ca XVII	192.85	6.75	-	-	-	0.08
	Ca XIV	193.87	6.55	-	-	0.04	-
	Fe XXIV	192.03	7.25	-	-	-	0.81
	Fe XII	195.12	6.2	0.08	0.18	0.17	-
	Fe XII	193.51	6.2	0.09	0.19	0.17	-
	Fe XII	192.39	6.2	0.04	0.09	0.08	-
	Fe XI	188.23	6.15	0.09	0.10	0.04	-
	Fe XI	192.83	6.15	0.05	0.06	-	-
	Fe XI	188.30	6.15	0.04	0.04	-	-
	Fe X	190.04	6.05	0.06	0.04	-	-
	Fe IX	189.94	5.85	0.06	-	-	-
	Fe IX	188.50	5.85	0.07	-	-	-
	Cont.			-	-	0.05	0.04
211 Å	Cr IX	210.61	5.95	0.07	-	-	-
	Ca XVI	208.60	6.7	-	-	-	0.09
	Fe XVII	204.67	6.6	-	-	-	0.07
	Fe XIV	211.32	6.3	-	0.13	0.39	0.12
	Fe XIII	202.04	6.25	-	0.05	-	-
	Fe XIII	203.83	6.25	-	-	0.07	-
	Fe XIII	209.62	6.25	-	0.05	0.05	-
	Fe XI	209.78	6.15	0.11	0.12	-	-
	Fe X	207.45	6.05	0.05	0.03	-	-
	Ni XI	207.92	6.1	0.03	-	-	-
	Cont.			0.08	0.04	0.07	0.41
304 Å	He II	303.786	4.7	0.33	0.32	0.27	0.29
	He II	303.781	4.7	0.66	0.65	0.54	0.58
	Ca XVIII	302.19	6.85	-	-	-	0.05
	Si XI	303.33	6.2	-	-	0.11	-
	Cont.			-	-	-	-
335 Å	Al X	332.79	6.1	0.05	0.11	-	-
	Mg VIII	335.23	5.9	0.11	0.06	-	-
	Mg VIII	338.98	5.9	0.11	0.06	-	-
	Si IX	341.95	6.05	0.03	0.03	-	-
	Si VIII	319.84	5.95	0.04	-	-	-
	Fe XVI	335.41	6.45	-	-	0.86	0.81
	Fe XIV	334.18	6.3	-	0.04	0.04	-
	Fe X	184.54	6.05	0.13	0.15	-	-
	Cont.			0.08	0.05	-	0.06

O'Dwyer, Del Zanna, Mason & Weber (A&A 2010), using the CHIANTI atomic package

Geometrical Interpretation of Problem

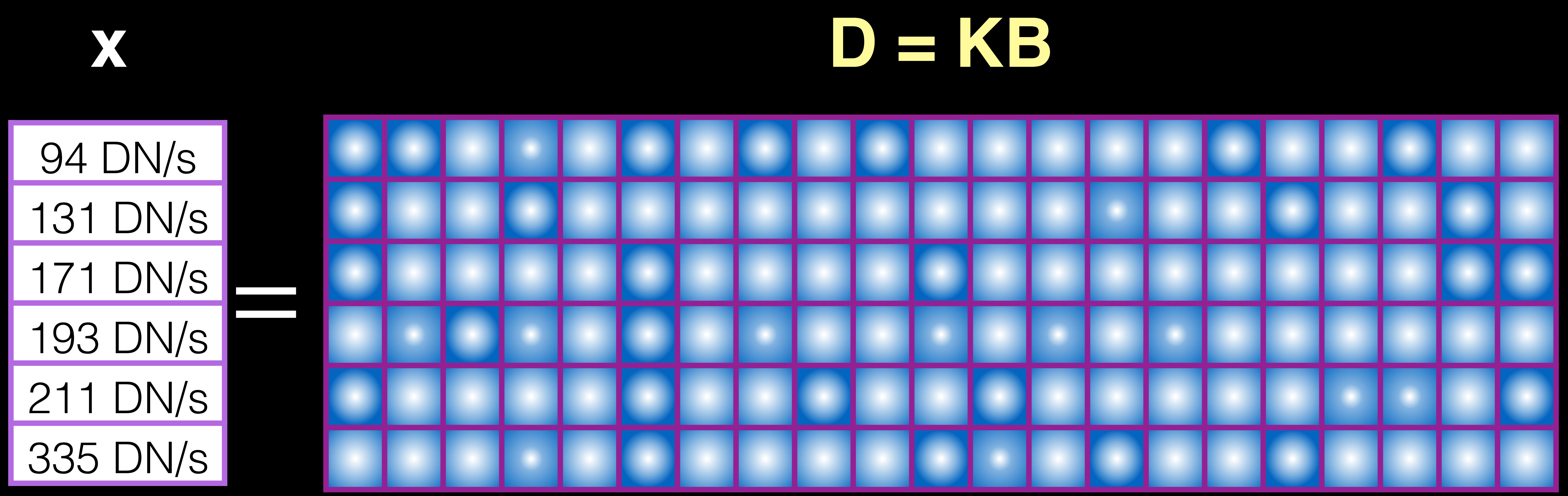

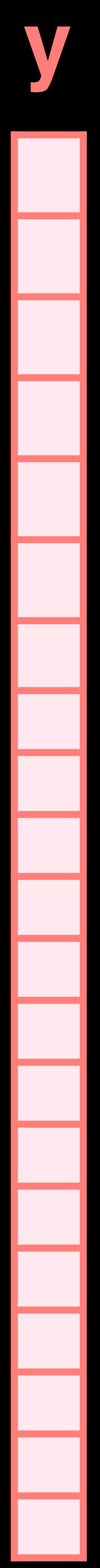

We seek to build a column vector **x** by linear combinations of columns of the matrix **D=KB**.

y_j are the coefficients of the linear combination.

More columns of **KB** from which to chose than components of x.

➔ underdetermined problem.

Do basis pursuit by minimizing L1 norm of y.

(Chen, Donoho & Saunders, SIAM Review, 2001)

We are seeking to solve for y

Sparse Inversion by Basis Pursuit

Choose a `simple' solution.

1) It tends not to overfit (consistent with the principle of parsimony, i.e. Ockham's Razor).
2) It ensures positivity of the solution (if solutions exist).
3) It is an L1-norm minimization problem, so we can use standard techniques from compressed sensing (see works by Donoho, Candes and Tao).

   BTW the L1-norm of a vector y = $\Sigma |y_i|$

4) Speed: O(10^4) solutions / sec with single thread running the IDL package.

Cheung et al. (2015), http://tinyurl.com/aiadem

χ2 minimization methods:

Parameterization: e.g. Guennou et al (2012a,b), Cheng et al (2012)

Regularization: e.g. Hannah & Kontar (2012), Plowman et al. (2013)

See Aschwanden et al. (2015, Sol Phys, 290, 2, 2733) for comparisons between methods.

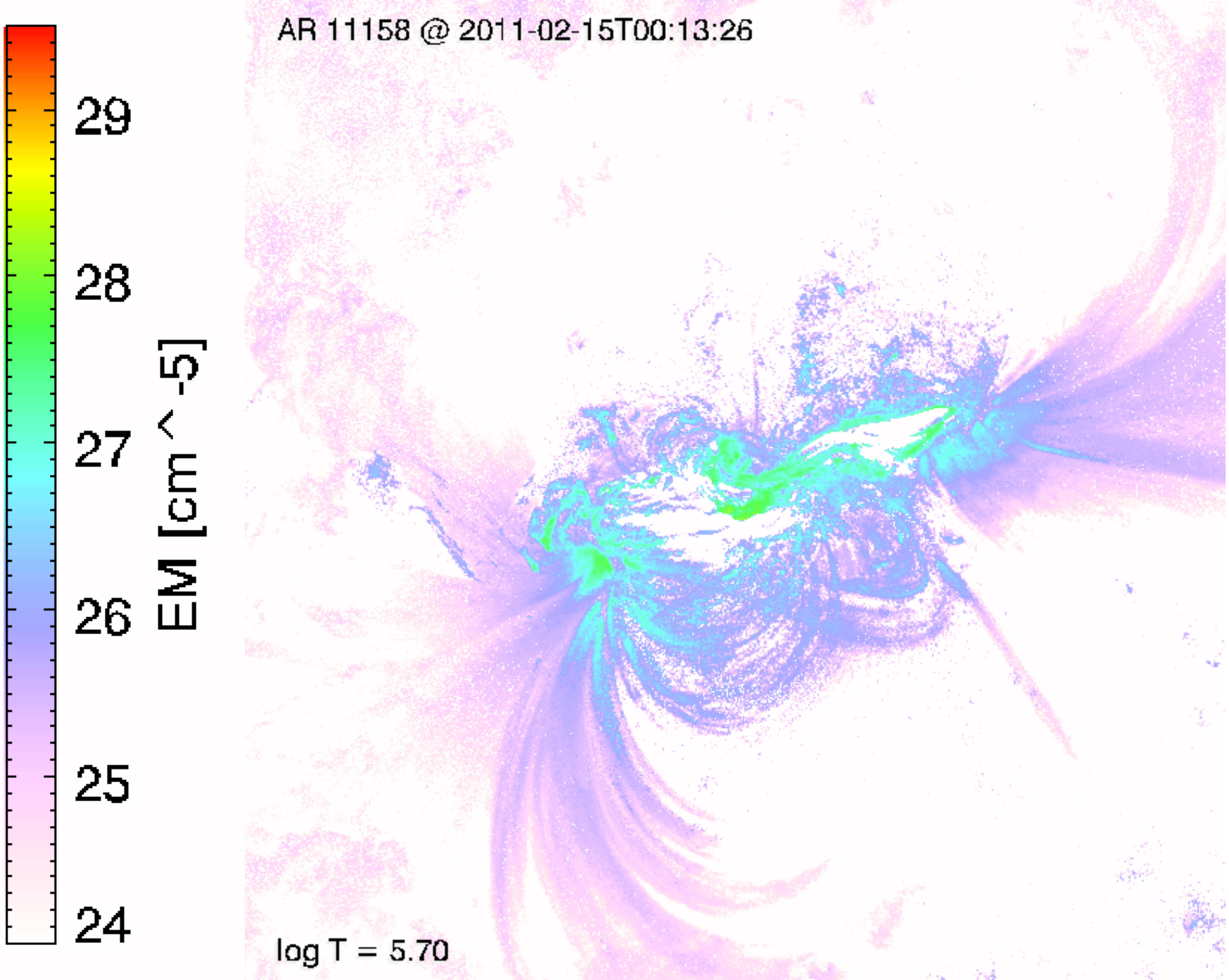

AR 11158 @ 2011-02-15T00:13:26
29
28
27
26
25
24
EM [cm ^ -5]
log T = 5.70

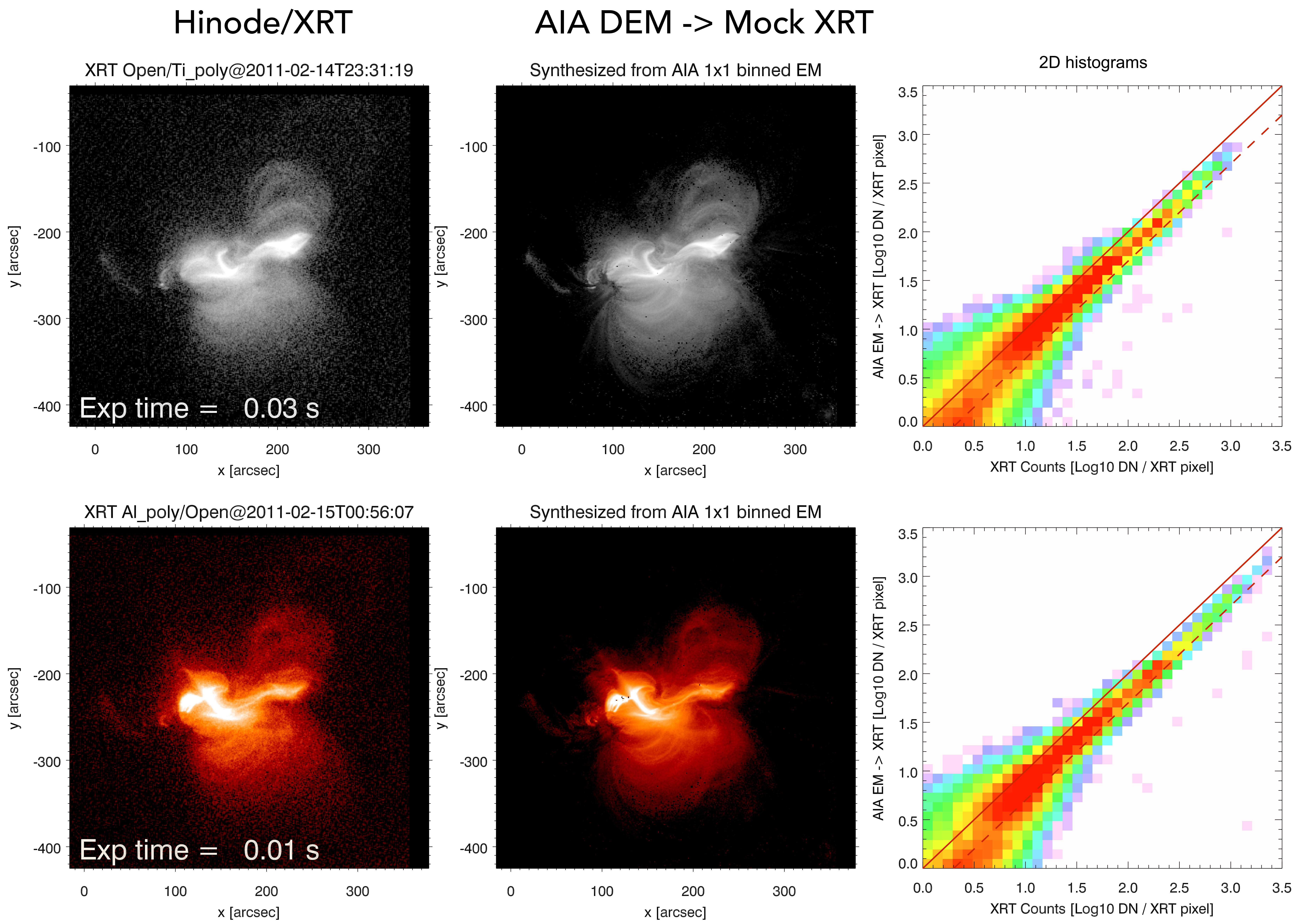

Also, see Su et al. (2018) for validation against RHESSI.

Flares: Models vs Observations

A *fluid* view of MHD

Magnetohydrodynamics (MHD) captures the following physical principles:

- Mass conservation, $\frac{D\varrho}{Dt} + \varrho\nabla\cdot\mathbf{v} = 0\,,$
- Momentum conservation,

$$\varrho\frac{D\mathbf{v}}{Dt} = \nabla\cdot\sigma + \varrho\mathbf{g},$$

$$\sigma_{ij} = -p\delta_{ij} + M_{ij},$$

$$M_{ij} = -\frac{B^2}{8\pi}\delta_{ij} + \frac{B_iB_j}{4\pi}.$$

- Energy conservation, $\varrho\frac{Ds}{Dt} = \frac{Q}{T}\,,$
- Faraday's law of induction. (next slide)

*Assumptions about material properties

Faraday's Induction Equation

Faraday's induction equation is

$$\frac{\partial \mathbf{B}}{\partial t} = -c\nabla \times \mathbf{E}\,, \tag{8}$$

where $\mathbf{E}$ is the electric field and c is the speed of light. In the regime of ideal MHD where the plasma is a perfect electrical conductor the electric field $\mathbf{E}'$ in the co-moving inertial frame of the plasma vanishes. Assuming the plasma velocity $\mathbf{v}$ has speed $|v| \ll c$, a Lorentz transformation to the 'lab' frame leads to

$$\mathbf{E} = -c^{-1}\mathbf{v} \times \mathbf{B}\,. \tag{9}$$

This yields the familiar Eulerian form of the ideal MHD induction equation

$$\frac{\partial \mathbf{B}}{\partial t} = \nabla \times (\mathbf{v} \times \mathbf{B})\,. \tag{10}$$

In Lagrangian form, this equation becomes

$$\frac{D\mathbf{B}}{Dt} = -\mathbf{B}(\nabla \cdot \mathbf{v}) + (\mathbf{B} \cdot \nabla)\mathbf{v}\,. \tag{11}$$

*Assumptions about material properties

Fluid expansion / compression

Stretching flow along magnetic field lines intensifies B

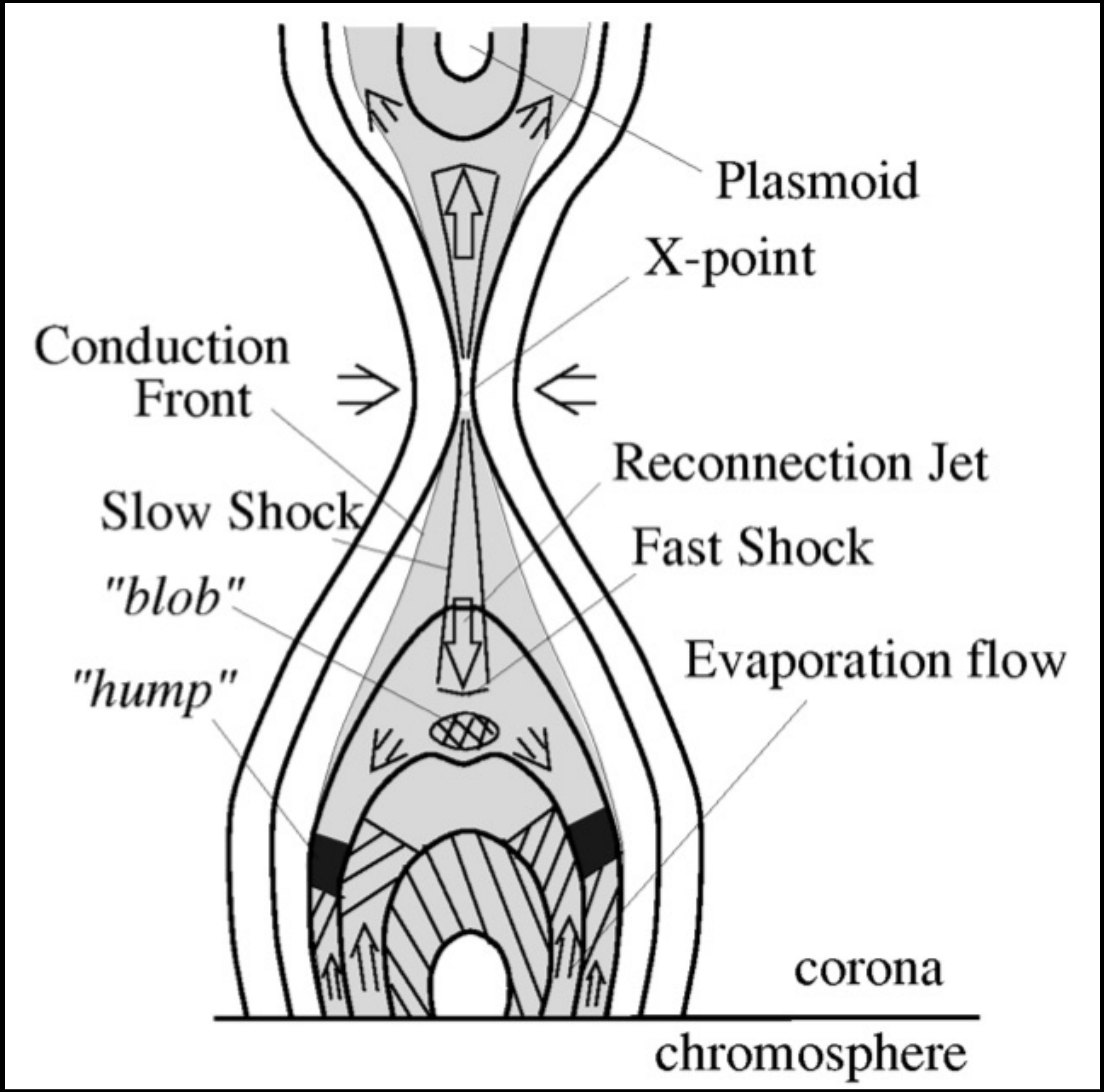

Yokoyama & Shibata (1998)

- 2D MHD model of flare reconnection.
- The efficient transport of energy released by reconnection is modeled as thermal conduction carried by electrons streaming along field lines.
- Energy dumped into the chromosphere leads to dense upflows (humps): "chromospheric evaporation"
- The model predicts density enhancement in the termination region.

Evolution of the thermal structure of a solar flare

M7.7 limb flare

- Patsourakos, Vourlidas & Stenborg, 2013, *ApJ*, **764**, 125
- Wei Liu, Chen & Petrosian, 2013, *ApJ*, **767**, 168
- Rui Liu, 2013, *MNRAS*, **434**, 1309
- Krücker & Battaglia , 2014, *ApJ*, **780**, 107
- Sun, Cheng & Ding, 2014, *ApJ*, **786**, 73
- Krücker et al., 2015, *ApJ*, **802**, 19

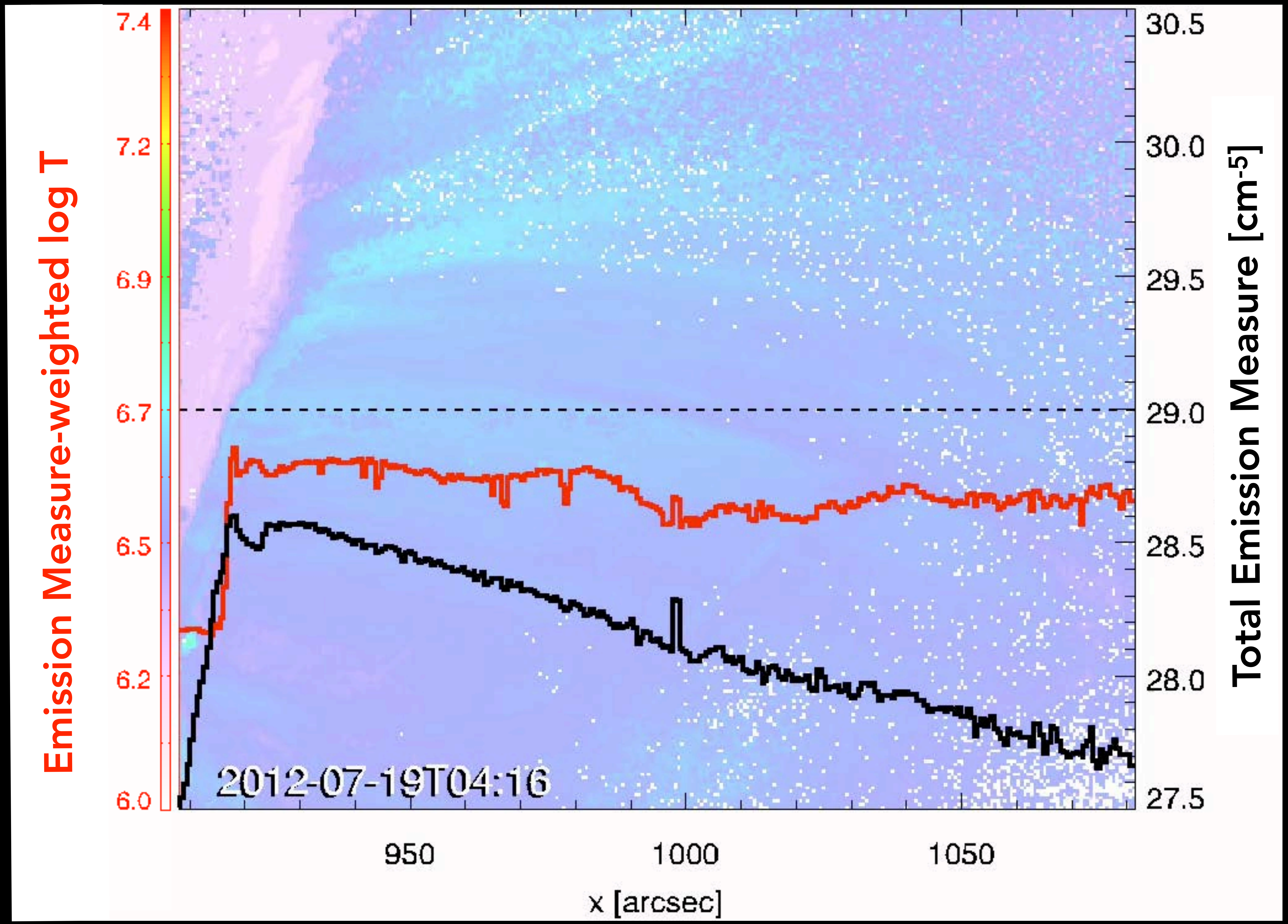

Evolution of the thermal structure of a solar flare

M7.7 limb flare

- Patsourakos, Vourlidas & Stenborg, 2013, *ApJ*, **764**, 125
- Wei Liu, Chen & Petrosian, 2013, *ApJ*, **767**, 168
- Rui Liu, 2013, *MNRAS*, **434**, 1309
- Krücker & Battaglia , 2014, *ApJ*, **780**, 107
- Sun, Cheng & Ding, 2014, *ApJ*, **786**, 73
- Krücker et al., 2015, *ApJ*, **802**, 19

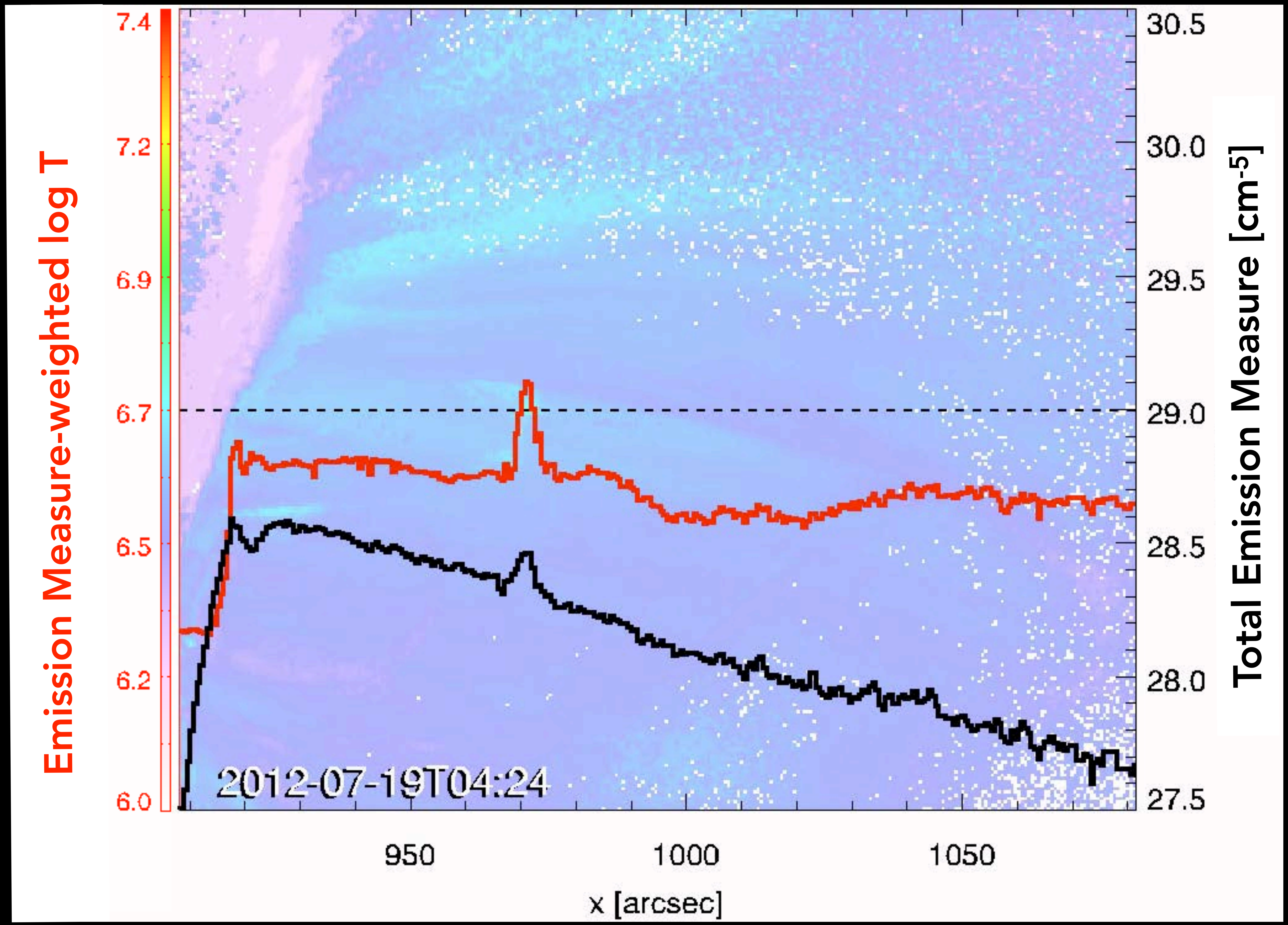

Evolution of the thermal structure of a solar flare

M7.7 limb flare

- Patsourakos, Vourlidas & Stenborg, 2013, *ApJ*, 764, 125
- Wei Liu, Chen & Petrosian, 2013, *ApJ*, 767, 168
- Rui Liu, 2013, *MNRAS*, 434, 1309
- Krücker & Battaglia , 2014, *ApJ*, 780, 107
- Sun, Cheng & Ding, 2014, *ApJ*, 786, 73
- Krücker et al., 2015, *ApJ*, 802, 19

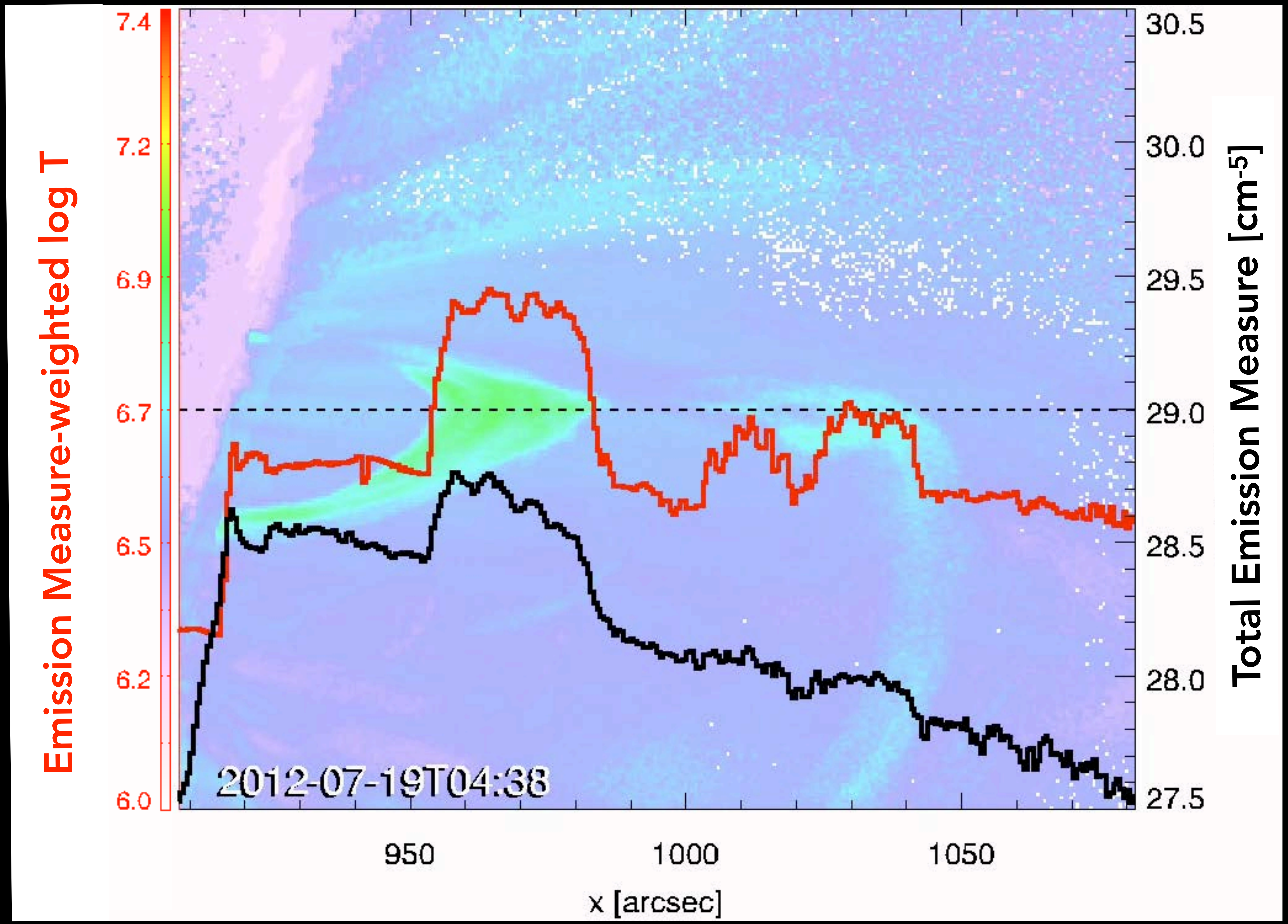

Evolution of the thermal structure of a solar flare

M7.7 limb flare

- Patsourakos, Vourlidas & Stenborg, 2013, *ApJ*, **764**, 125
- Wei Liu, Chen & Petrosian, 2013, *ApJ*, **767**, 168
- Rui Liu, 2013, *MNRAS*, **434**, 1309
- Krücker & Battaglia , 2014, *ApJ*, **780**, 107
- Sun, Cheng & Ding, 2014, *ApJ*, **786**, 73
- Krücker et al., 2015, *ApJ*, **802**, 19

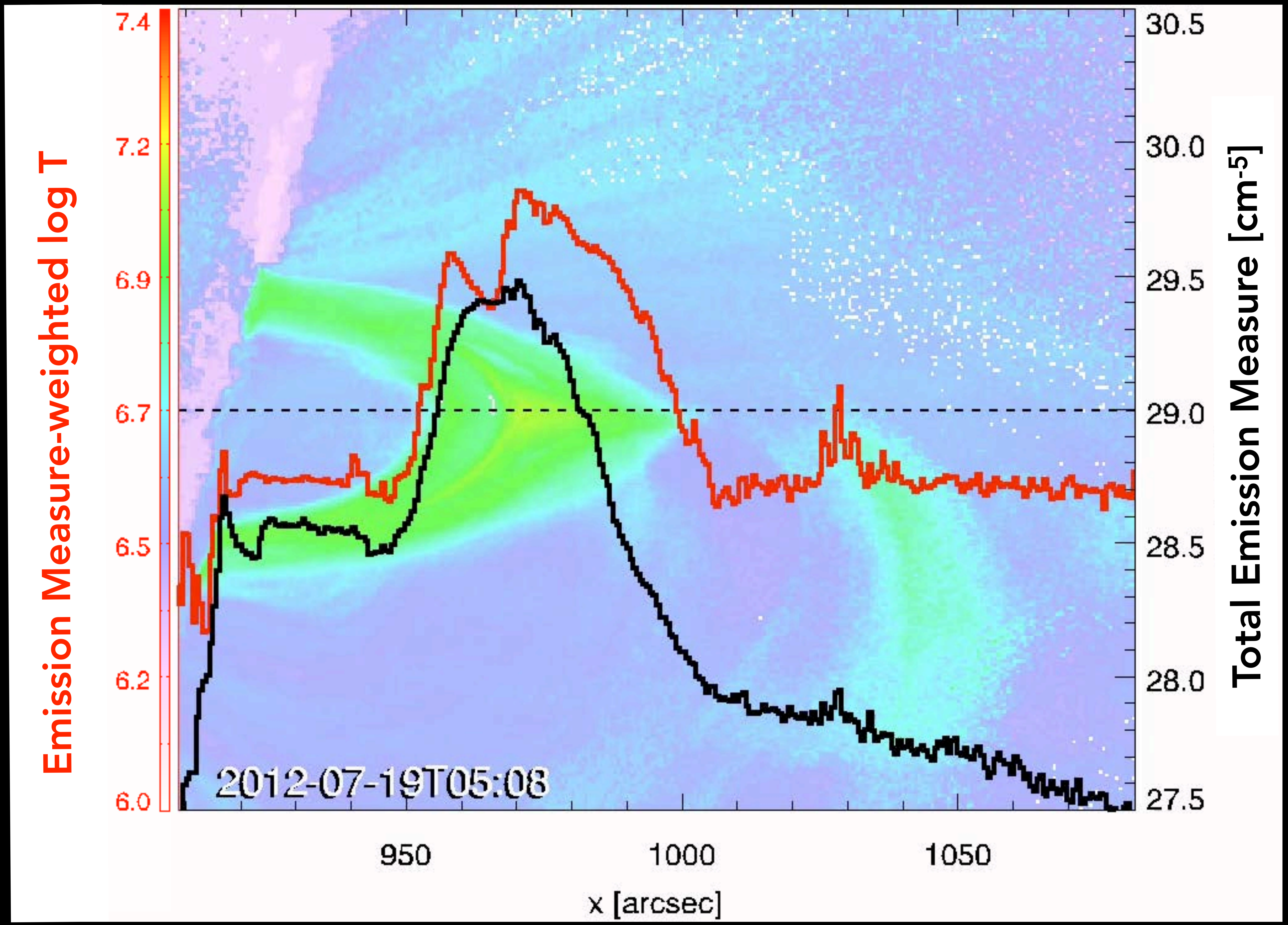

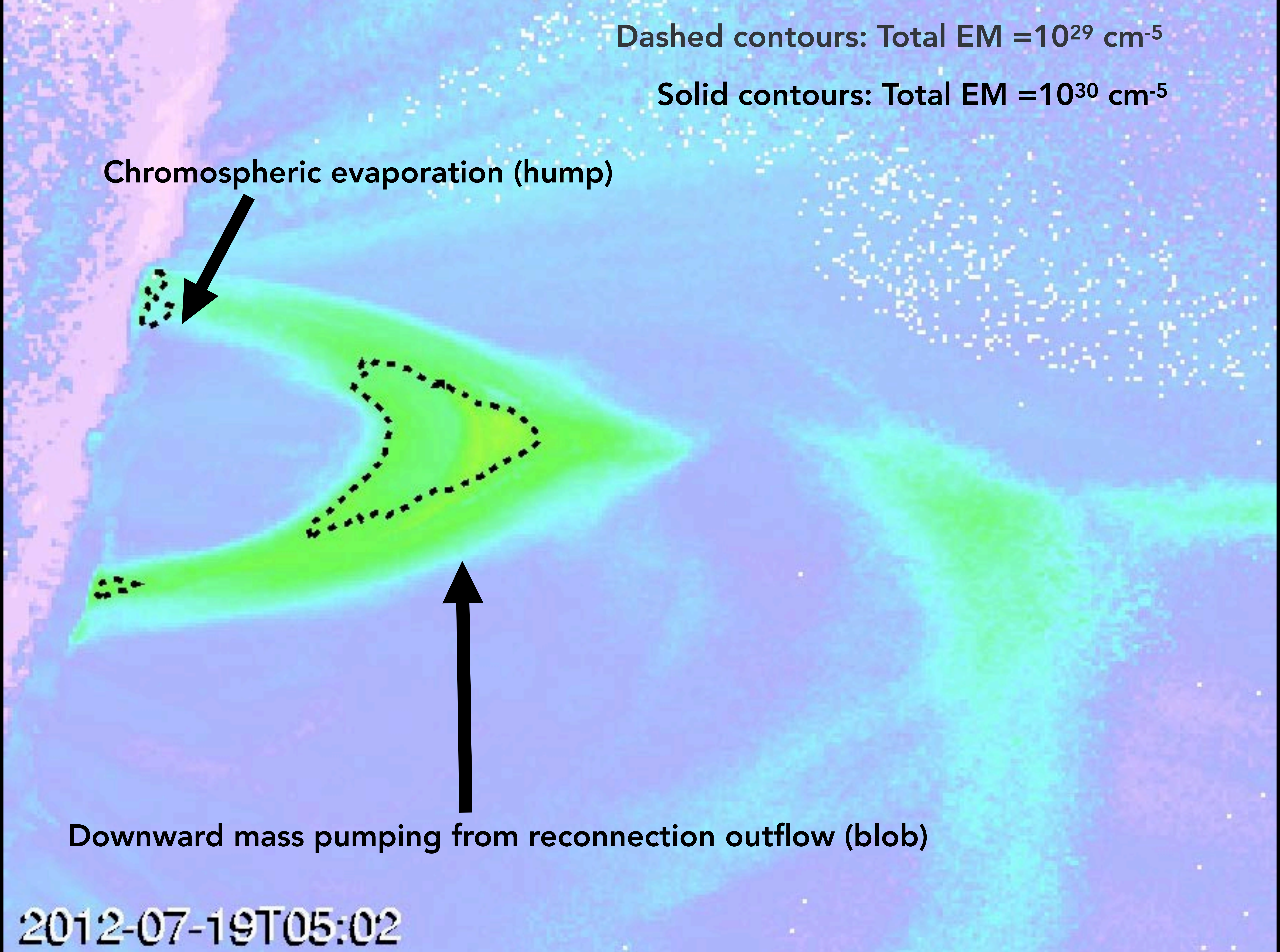

Dashed contours: Total EM =10^29 cm^-5
Solid contours: Total EM =10^30 cm^-5
Chromospheric evaporation (hump)
Downward mass pumping from reconnection outflow (blob)
2012-07-19T05:02

MHD Simulation of a Solar Flare (Cheung, Rempel et al. 2019)

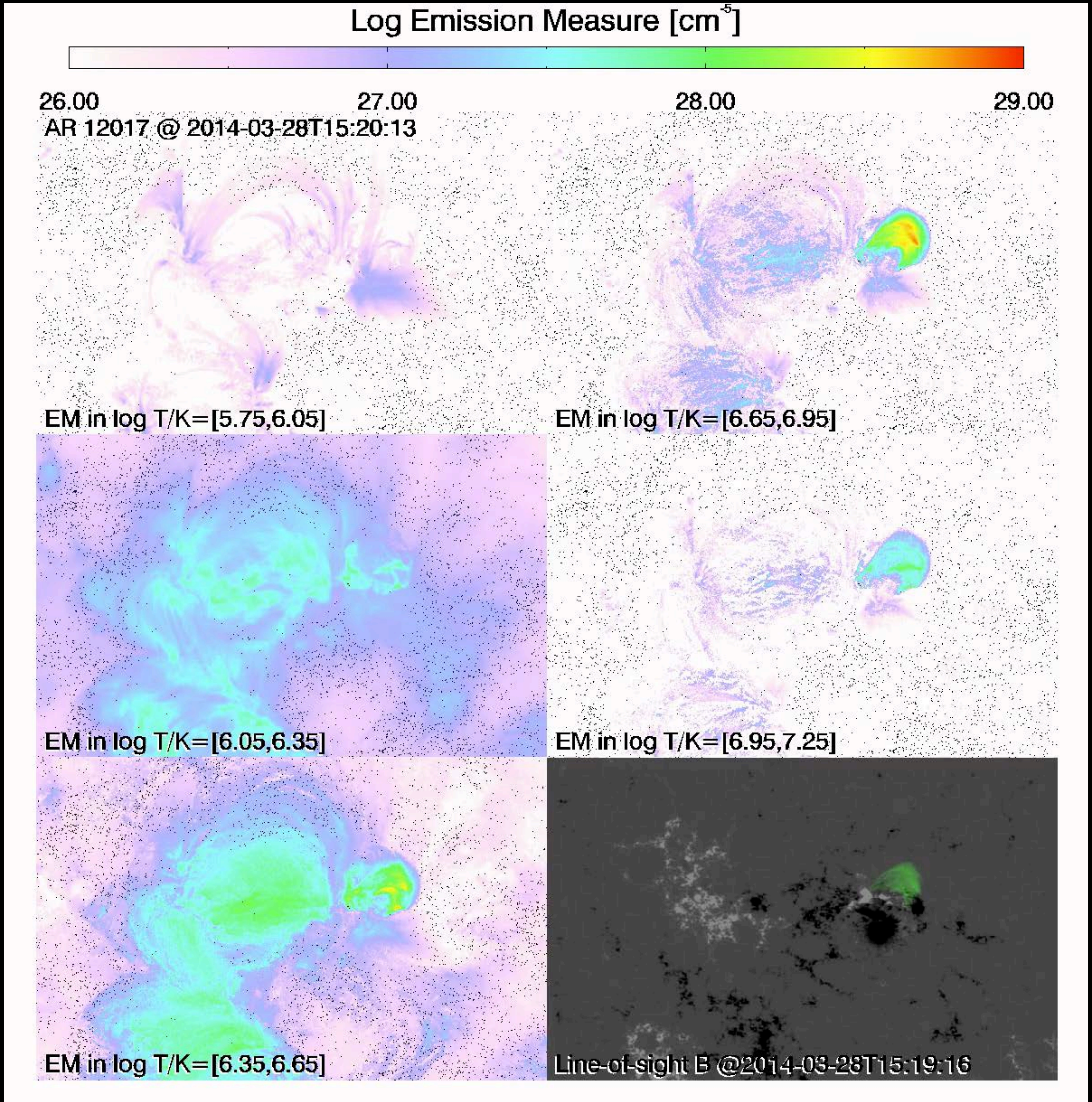

NOAA AR 12017:
one X-class ("Best Observed X-flare"), 3 M-class, and about two dozen C-class flares

Sunquake: Judge et al. (2014)
Filament Eruption before X-flare: Kleint et al. (2015)
IRIS Fe XXI FUV spectra: Young et al. (2015)
Chromospheric Evaporation: Li et al. (2015)

Synthetic GOES X-ray Light Curves

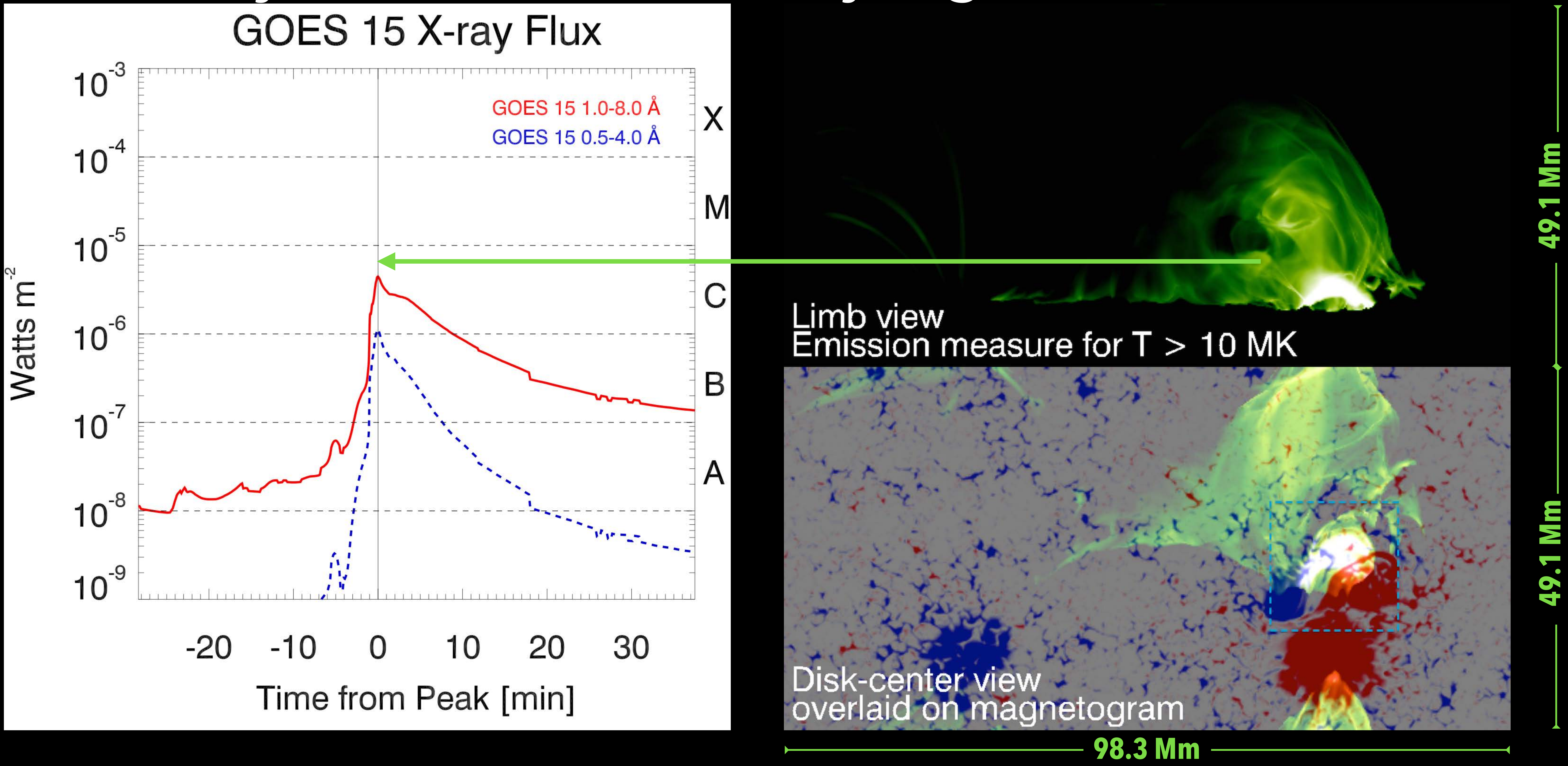

C4 flare if measured by detectors on GOES 15. The free magnetic energy (actual minus potential field) dropped by ~5x10^{30} erg (~10%) over 5 minutes.

Using using thermal bremsstrahlung, the model yields power law-like shapes for the X-ray spectrum (eg. RHESSI).

The multi-thermal nature of the magnetic structure gives rise to the apparent non-thermal behavior.

Above-the-loop-top harder X-ray sources (> 25 keV) are located above softer loop sources.

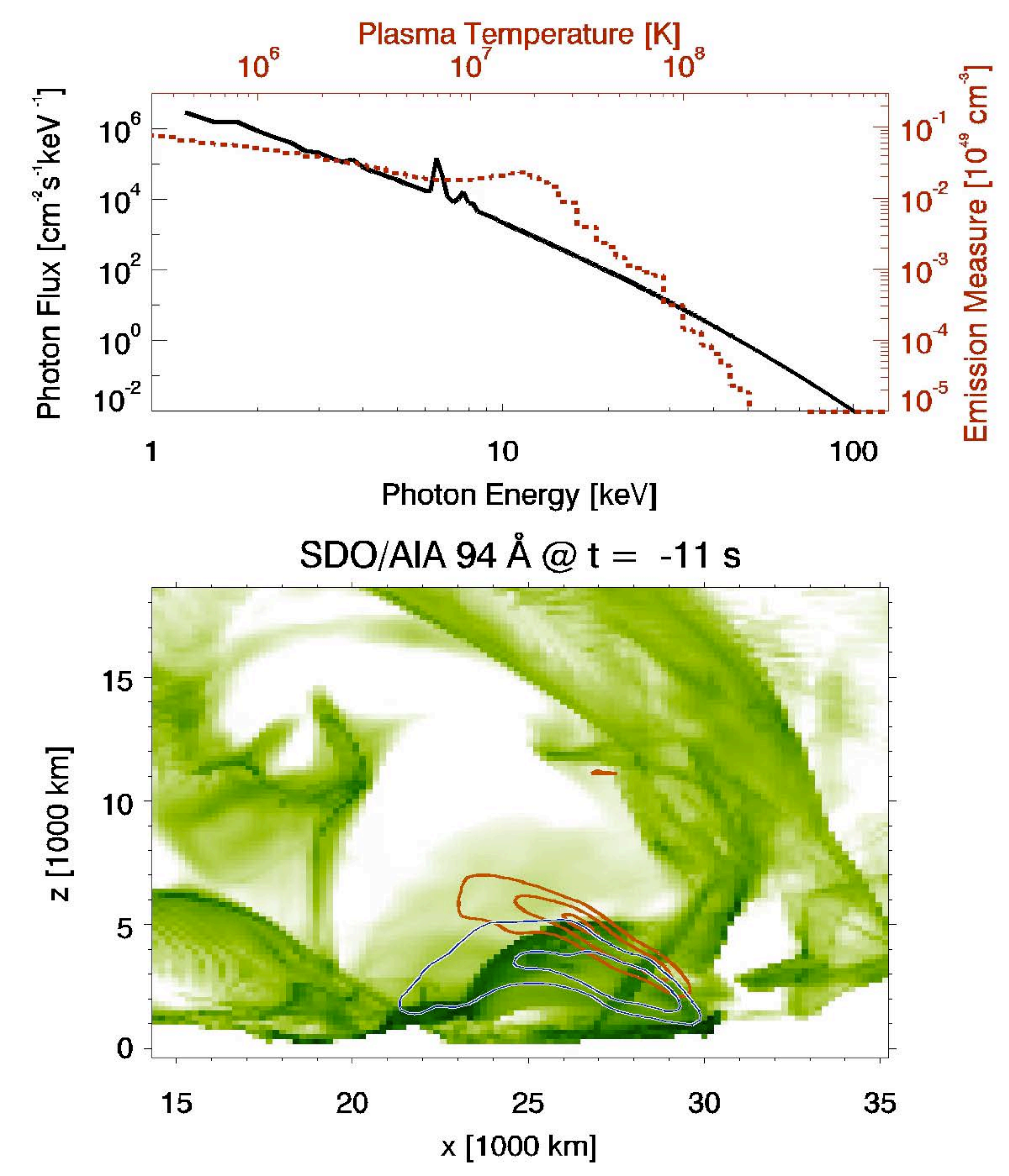

Hard x-rays ≥ 25 keV 6 ≤ Soft x-rays ≤ 12 keV

Using using thermal bremsstrahlung, the model yields power law-like shapes for the X-ray spectrum (eg. RHESSI).

The multi-thermal nature of the magnetic structure gives rise to the apparent non-thermal behavior.

Above-the-loop-top harder X-ray sources (> 25 keV) are located above softer loop sources.

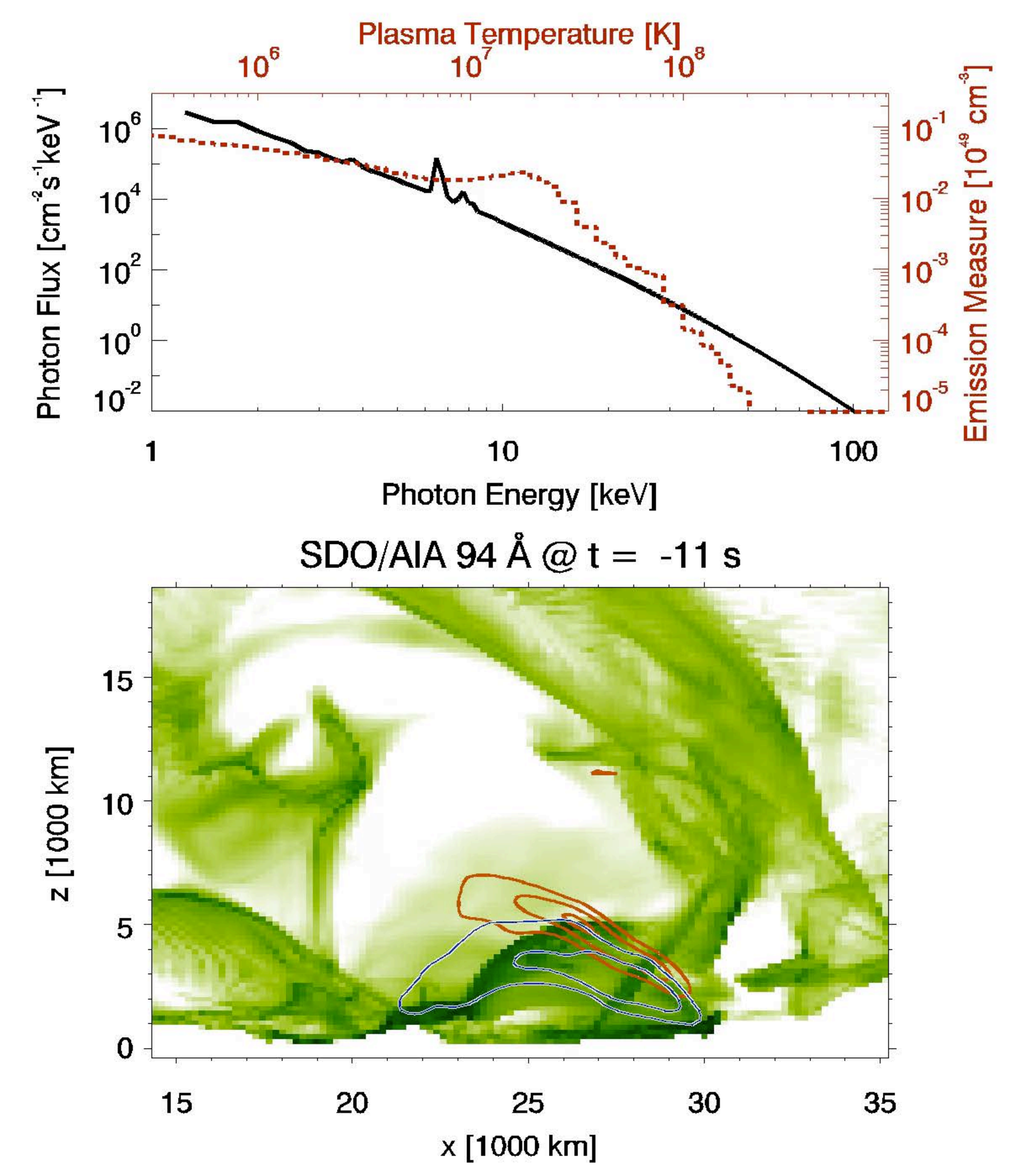

Hard x-rays ≥ 25 keV   6 ≤ Soft x-rays ≤ 12 keV

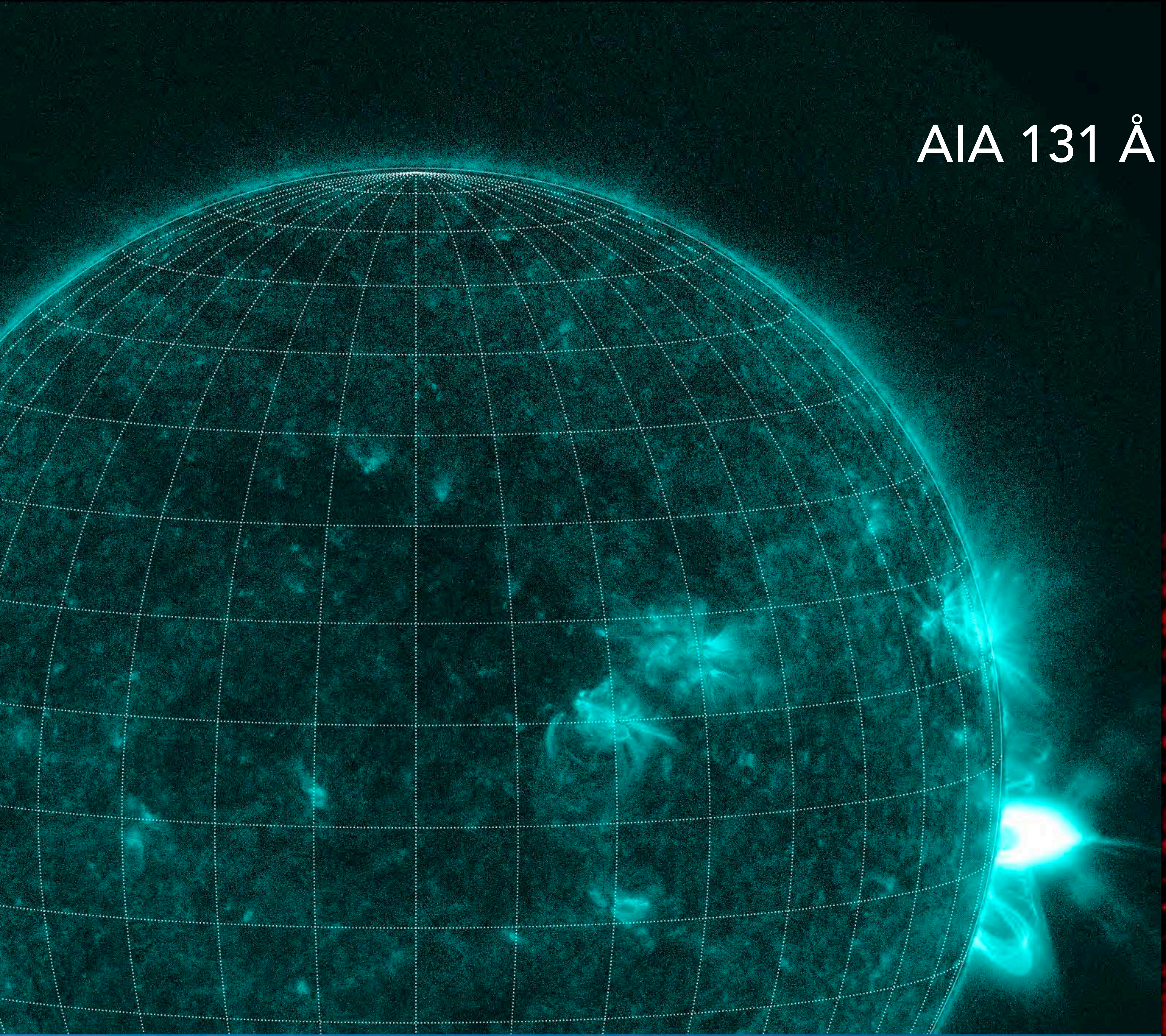
AIA 131 Å


Expanded Owens Valley Solar Array (EOVSA)

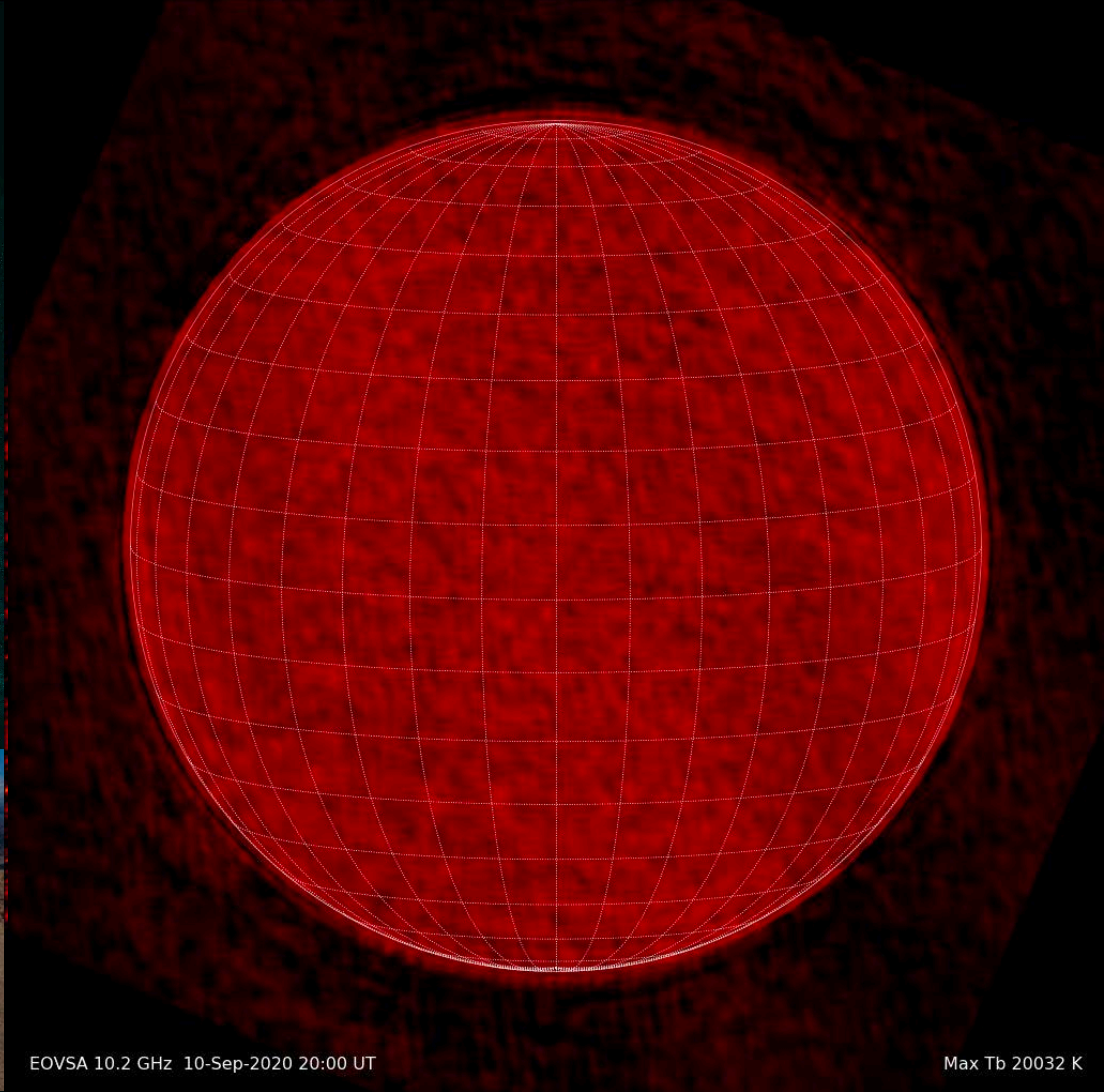
EOVSA 10.2 GHz 10-Sep-2020 20:00 UT
Max Tb 20032 K

Expanded Owens Valley Solar Array (EOVSA) Chen et al, Nature Astronomy, 2020

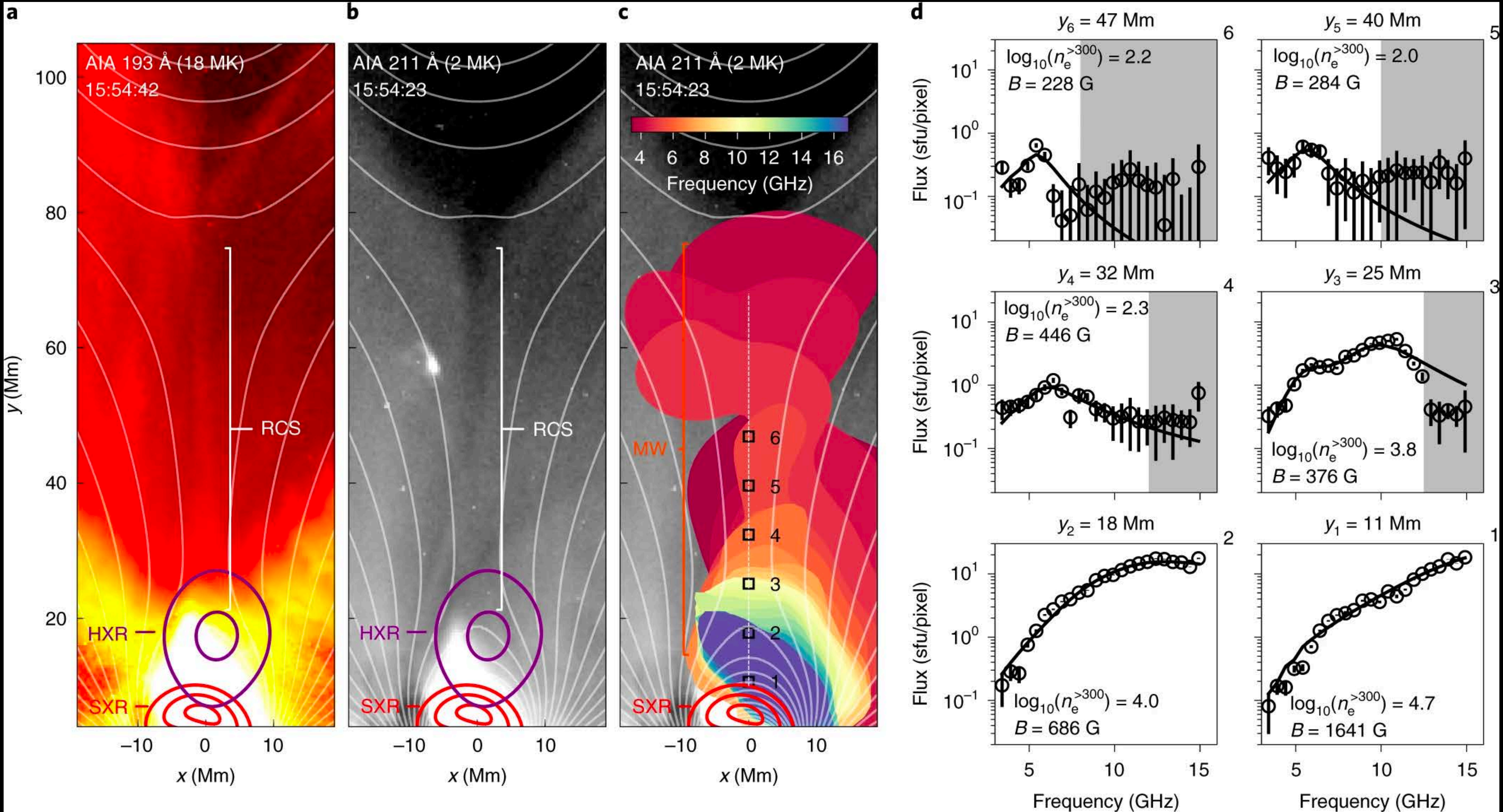

Next Generation Solar Physics Mission (NGSPM)

The NSGPM is a mission concept developed by a panel of solar physics experts designated by NASA, ESA and JAXA. The NGSPM report prioritizes a mission with the following suite of observing capabilities:

0.3″ coronal / TR spectrograph	**0.2″ - 0.6″ coronal imager**	**0.1″ - 0.3″ chromospheric photospheric magnetograph / spectrograph**
Solar-C_EUVST	MUSE MULTISLIT SOLAR EXPLORER	DKIST DANIEL K. INOUYE SOLAR TELESCOPE **+GBOs**

Coordinated observations are an integral part of the MUSE investigation. **Coordination of MUSE with EUVST+Ground Based Observatories (GBOs such as DKIST) will address multiple NGSPM science objectives** (see De Pontieu et al. 2022; Cheung et al. 2022).

Take home message

Go for the Total Eclipse

Other references

- *Solar Irradiances*, Kopp, 2017 https://heliophysics.ucar.edu/sites/default/files/heliophysics/resources/presentations/2017_Kopp_Solar_Irradiances.pdf
- *Why Does the Sun have a Corona? And a Wind?* Longcope, 2018 https://heliophysics.ucar.edu/sites/default/files/heliophysics/resources/presentations/2018_Loncope_Corona.pdf
- Spectrolarimetry / Zeeman effect: Borrero (2004, PhD thesis; Chapter 1), https://www.mps.mpg.de/phd/theses/the-fine-structure-of-the-sunspot-penumbra.pdf
- Radiative hydrodynamics in the solar atmosphere: Leenaarts (Living Reviews in Solar Physics, 2020) https://link.springer.com/article/10.1007/s41116-020-0024-x
- Photosphere to Chromosphere to Coronal Coupling: Wedemeyer-Böhm, Lagg & Nordlund (2009) https://link.springer.com/article/10.1007/s11214-008-9447-8
- **Downloading and plotting a HMI magnetogram using sunpy:** https://docs.sunpy.org/en/stable/generated/gallery/acquiring_data/downloading_hmi.html
- **aiapy,** https://aiapy.readthedocs.io/en/stable/generated/gallery/index.html
- **Downloading AIA and HMI data direct from the source (SDO Joint Science Ops Center, JSOC):** http://jsoc.stanford.edu/ajax/lookdata.html
- **Radiative Processes in Flares I: Bremsstrahlung, Chen:** https://web.njit.edu/~binchen/phys780/LectureNotes/lec20.pdf
- **Radiative Processes From Energetic Particles II: Gyromagnetic Radiation, Chen:** https://web.njit.edu/~binchen/phys780/LectureNotes/lec21.pdf